Article

Cell Reports

In Vivo Protein Complementation Demonstrates Presynaptic α-Synuclein Oligomerization and Age-Dependent Accumulation of 8–16-mer Oligomer Species

Graphical Abstract

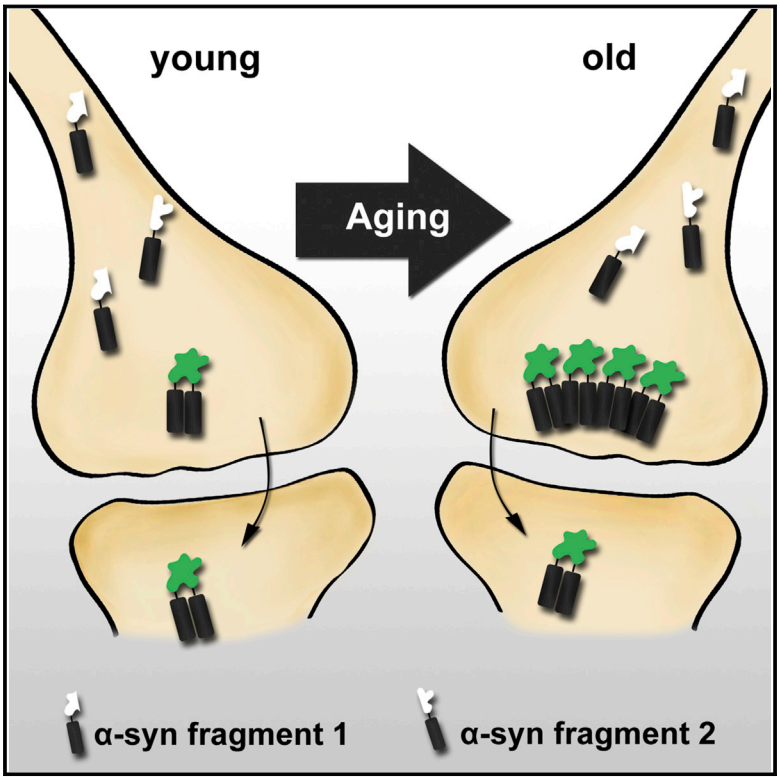

Highlights

- Inducible split protein mouse models to quantify α-synuclein oligomerization *in vivo*
- Aging promotes accumulation of size-defined α-synuclein oligomers
- α-synuclein oligomerization takes place at the presynapse
- Cell-to-cell transmission of α-synuclein is demonstrated in an intact mouse brain

Authors

Martin Kiechle, Bjoern von Einem, Lennart Höfs, ..., Björn H. Falkenburger, Jochen H. Weishaupt, Karin M. Danzer

Correspondence

karin.danzer@uni-ulm.de

In Brief

Kiechle et al. present two transgenic mouse models that allow direct quantitative and spatial detection of α-synuclein (α-syn) oligomers *in vivo*. They demonstrate α-syn aggregation at the synapse, age-dependent accumulation of 8–16-mer α-syn oligomer species, and trans-cellular oligomer spreading from forebrain to hindbrain neurons.

Kiechle et al., 2019, Cell Reports *29*, 2862–2874
November 26, 2019 © 2019 The Author(s).
https://doi.org/10.1016/j.celrep.2019.10.089

CellPress

OPEN ACCESS
CellPress

Cell Reports
Article

In Vivo Protein Complementation Demonstrates Presynaptic α-Synuclein Oligomerization and Age-Dependent Accumulation of 8–16-mer Oligomer Species

Martin Kiechle,[1] Bjoern von Einem,[1] Lennart Höfs,[2] Patrizia Voehringer,[3] Veselin Grozdanov,[1] Daniel Markx,[4] Rosanna Parlato,[5] Diana Wiesner,[1] Benjamin Mayer,[6] Olena Sakk,[7] Bernd Baumann,[7] Soeren Lukassen,[8] Birgit Liss,[5,10] Arif B. Ekici,[8] Albert C. Ludolph,[1] Paul Walther,[9] Boris Ferger,[3] Pamela J. McLean,[11] Björn H. Falkenburger,[2] Jochen H. Weishaupt,[1] and Karin M. Danzer[1,12,*]

[1]Department of Neurology, Ulm University, Ulm, Germany
[2]Department of Neurology, Dresden University Medical Center, Dresden, Germany
[3]CNS Diseases Research, Boehringer Ingelheim Pharma GmbH & Co. KG, Biberach, Germany
[4]Institute of Protein Biochemistry, Ulm University, Ulm, Germany
[5]Institute of Applied Physiology, Ulm University, Ulm, Germany
[6]Institute of Epidemiology and Medical Biometry, Ulm University, Ulm, Germany
[7]Institute of Physiological Chemistry, Ulm University, Ulm, Germany
[8]Institute of Human Genetics, Friedrich-Alexander-University of Erlangen-Nürnberg, Erlangen, Germany
[9]Central Facility for Electron Microscopy, Ulm University, Ulm, Germany
[10]New College, University of Oxford, Oxford OX1 3BN, UK
[11]Department of Neuroscience, Mayo Clinic, Jacksonville, FL 32224, USA
[12]Lead Contact
*Correspondence: karin.danzer@uni-ulm.de
https://doi.org/10.1016/j.celrep.2019.10.089

SUMMARY

Intracellular accumulation of α-synuclein (α-syn) and formation of Lewy bodies are neuropathological characteristics of Parkinson's disease (PD) and related α-synucleinopathies. Oligomerization and spreading of α-syn from neuron to neuron have been suggested as key events contributing to the progression of PD. To directly visualize and characterize α-syn oligomerization and spreading *in vivo*, we generated two independent conditional transgenic mouse models based on α-syn protein complementation assays using neuron-specifically expressed split Gaussia luciferase or split Venus yellow fluorescent protein (YFP). These transgenic mice allow direct assessment of the quantity and subcellular distribution of α-syn oligomers *in vivo*. Using these mouse models, we demonstrate an age-dependent accumulation of a specific subtype of α-syn oligomers. We provide *in vivo* evidence that, although α-syn is found throughout neurons, α-syn oligomerization takes place at the presynapse. Furthermore, our mouse models provide strong evidence for a transsynaptic cell-to-cell transfer of *de novo* generated α-syn oligomers *in vivo*.

INTRODUCTION

Parkinson's disease (PD) is a progressive neurodegenerative disease with age being the strongest risk factor. Loss of dopaminergic neurons in the substantia nigra and other parts of the nervous system together with the presence of intra-neuronal inclusions called Lewy bodies or Lewy neurites are main characteristics of PD. Aggregates of α-synuclein (α-syn) are the main component of Lewy bodies and Lewy neurites. α-Syn is closely linked to PD pathogenesis since several mutations in α-syn (A30P, E46K, A53T, A53E, G51D, and H50Q) or solely increased gene dosage of α-syn are sufficient to cause familial forms of PD (Rosborough et al., 2017).

Although the exact mechanism of α-syn toxicity remains unknown, accumulating evidence suggests that the precursors of deposited α-syn, oligomers and fibrils, are the toxic species in PD (Dehay et al., 2015; Fusco et al., 2017; Winner et al., 2011; Auluck et al., 2010). Moreover, post-translational modifications including C-terminal cleavage (Sung et al., 2005), oxidation, nitration (Hodara et al., 2004), and phosphorylation (Fujiwara et al., 2002; Paleologou et al., 2010) might contribute to oligomerization, fibrillization, and toxicity (Barrett and Timothy Greenamyre, 2015).

α-Syn assemblies released from neurons can propagate in a prion-like manner by seeding aggregation of endogenous α-syn in neighboring cells. Several *in vitro* (exposure of cells to α-syn oligomers or fibrils) and *in vivo* experiments (injection of synthetic preformed fibrils or brain homogenates derived from diseased mice or from PD patients, cell transplantations, and viral overexpression of α-syn) support seeded aggregation and interneuronal transmission of α-syn (Danzer et al., 2007, 2009, 2011; Desplats et al., 2009; Hansen et al., 2011; Volpicelli-Daley et al., 2011; Luk et al., 2012a, 2012b; Rey et al., 2013; Holmqvist et al., 2014; Ulusoy et al., 2013). These findings underline the observations by Braak et al. (2003), describing that α-syn inclusion body pathology in PD occurs in a hierarchical distribution, starting in the stomach and propagating to axonally connected areas.

While strategies to study spreading of α-syn *in vivo* were to date mainly based on exogenous injection of α-syn in mouse

 © 2019 The Author(s).
This is an open access article under the CC BY-NC-ND license (http://creativecommons.org/licenses/by-nc-nd/4.0/).

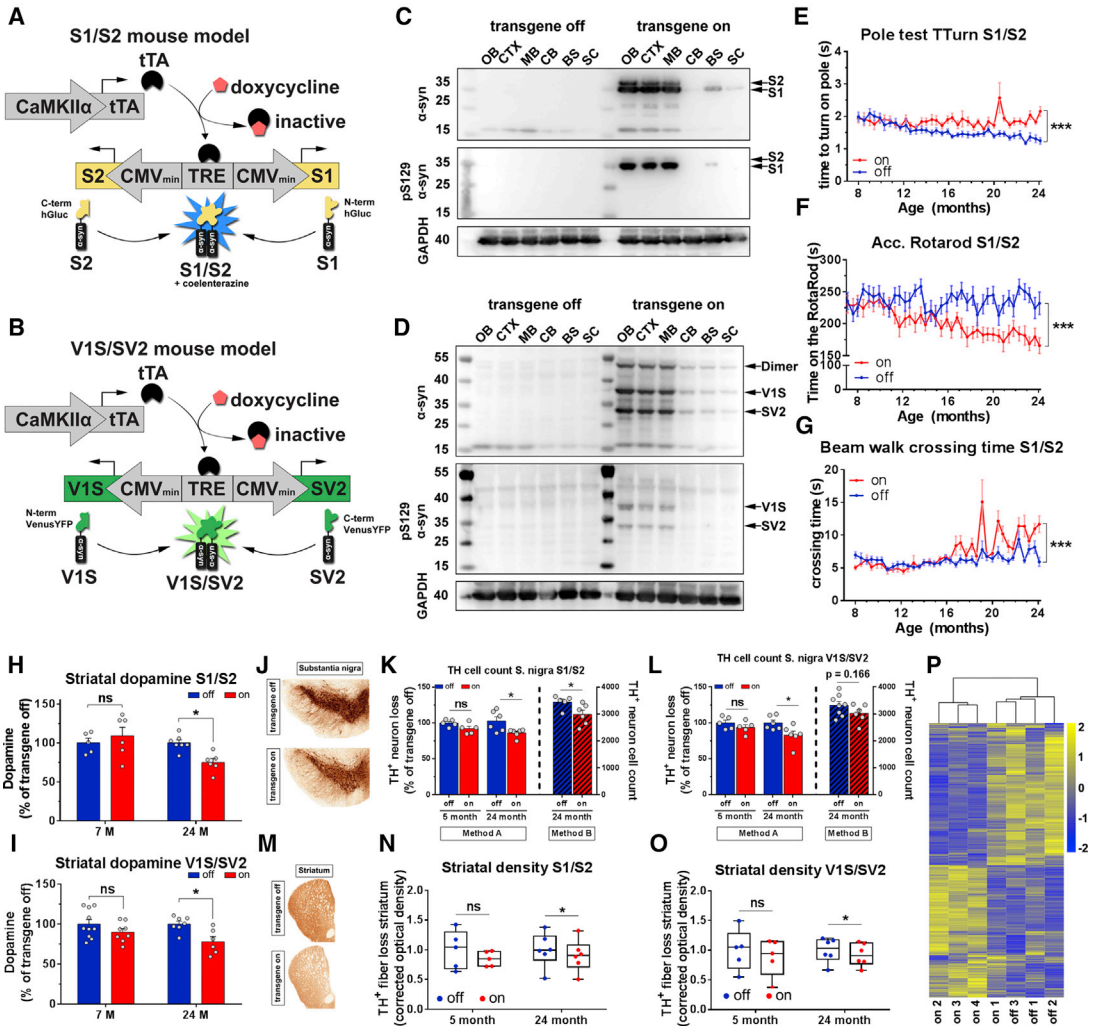

Figure 1. Characterization of Conditional S1/S2 and V1S/SV2 Mice

(A and B) Schematic diagram of the two conditional protein-fragment complementation assay (PCA) mouse models S1/S2 (A) and V1S/SV2 (B). Expression is driven by neuron specific CaMKIIα promoter in a Tet-off system. For S1/S2, human wild-type α-syn is tagged with either N- or C-terminal part of hGaussia luciferase. For V1S/SV2, Venus YFP halves are fused to α-syn.

(C and D) Western blot of 24-month-old S1/S2 (C) and V1S/SV2 (D) brains using α-syn clone 42 (BD) and pSyn#64 (WAKO) antibodies. Loading control: Glyceraldehyde-3-phosphate dehydrogenase (GAPDH). Brains were dissected according to Figure S1A. OB, olfactory bulb; CTX, cortex; MB, midbrain/basal ganglia; CB, cerebellum; BS, brainstem; and SC, spinal cord.

(E) Pole test analysis of S1/S2 animals showed age-associated motor impairment (n = 15 male mice; repeated-measures two-way ANOVA, ***$p \leq 0.001$). TTurn = time to turn and orientate downward on the pole. First significant impairments for TTurn were detected at 14.5 months (Mann-Whitney *U* test; $p < 0.05$). Data: mean ± SEM.

(F) Progressive aggravation in motor balance and coordination in S1/S2 animals (n = 15 male mice, repeated-measures two-way ANOVA, ***$p \leq 0.001$). First significant impairments were observed at 11.7 months (t test; $p < 0.05$). Data: mean ± SEM.

(G) Beam walk analysis revealed significant balance dysfunction in S1/S2 expressing mice during aging (n = 15 male mice, repeated-measures two-way ANOVA, ***$p \leq 0.001$). Earliest significant impairment was observed at 16.8 months (t test; $p < 0.05$). Data: mean ± SEM.

(H and I) Striatal dopamine concentration of S1/S2 (H) and V1S/SV2 (I) animals was measured by HPLC coupled with electrochemical detection (ECD). Significant reduction of dopamine was detected at 24 months for α-syn overexpressing mice (n = 6–10 mice per group and time point; two-way ANOVA with Sidak's post hoc test; *$p \leq 0.05$; ns = not significant). Bars: mean ± SEM.

(J) Representative tyrosine hydroxylase (TH) staining in the substantia nigra of V1S/SV2 mice.

(K and L) The number of TH-positive neurons was counted in the substantia nigra pars compacta of S1/S2 (K) and V1S/SV2 (L) mice using two different methods (please see STAR Methods for details). For method A, TH^+ cell loss was estimated at 5 (n = 5 mice per group) and 24 months of age (n = 6 mice per group), two-way ANOVA with Sidak's post hoc test, *$p \leq 0.05$, ns = not significant. For method B, TH^+ cell loss was stereologically counted in 24-month-old mice using the optical fractionator method (S1/S2: n = 5–6 mice per group, V1S/SV2: n = 6–8 mice per group). Two-tailed unpaired t test. All data: mean ± SEM.

(legend continued on next page)

brain, evidence for cell-to-cell spreading of α-syn in transgenic models is rare. We and others have previously demonstrated that protein-fragment complementation assays (PCAs) such as bimolecular fluorescence complementation or split luciferase reporter systems are powerful tools for studying protein-protein interactions and monitoring the formation of α-syn oligomers and aggregation directly *in vitro* and *in vivo* (Danzer et al., 2011; Putcha et al., 2010; Outeiro et al., 2008; Dimant et al., 2013; Cai et al., 2018; Delenclos et al., 2016; Aelvoet et al., 2014). We have now generated two human α-syn transgenic neuron-specific mouse models designed in a Tet-off system combined with a PCA, using a split luciferase and a split Venus YFP system.

With this experimental approach, we evaluated the effect of aging on α-syn oligomer formation, defined the cellular compartment of aggregation, and studied cell-to-cell spreading of α-syn *in vivo*. Furthermore, we determined neuropathological, neurochemical, and behavioral changes upon α-syn oligomer generation. Our transgenic mouse models are valuable tools for understanding the mechanistic interplay between aging, α-syn oligomerization, and spreading, which will promote new therapeutic approaches in PD.

RESULTS

Generation of α-Syn Oligomer Mice

In order to monitor α-syn oligomerization *in vivo* we made use of a bioluminescent protein complementation assay. To that end, the N-terminal and C-terminal halves of Gaussia luciferase were fused to wild-type (WT) human α-syn (named S1 and S2, respectively). Oligomerization of α-syn leads to reconstitution of Gaussia luciferase, resulting in the production of bioluminescence upon administration of the substrate coelenterazine. Moreover, for the development of a fluorescent PCA Venus YFP was fragmented into N- and C-terminal parts then fused each with WT α-syn to form non-fluorescent fusion proteins V1S and SV2, respectively. In analogy to bioluminescent PCA, non-fluorescent V1S and SV2 reconstitute to fluorescent Venus YFP when α-syn oligomerizes (Dimant et al., 2013; Danzer et al., 2011).

For *in vivo* application a transgenic mouse model with a tetracycline regulated S1 and S2 expression (Tet-off) was generated (Gossen and Bujard, 1992). S1 and S2 were placed under the control of a tetracycline response element (TRE) with a bidirectional CMV_{min} promoter, which regulates the expression of both S1 and S2. These single transgenic S1/S2 mice were then crossbred with the CaMKIIα-tTA driver line in order to induce S1 and S2 expression in neurons of different forebrain areas (Mayford et al., 1996a) (Figure 1A). To avoid any transgene expression during embryonic development, animals were bred and housed in the presence of doxycycline (dox) until birth.

Analogous to the WT α-syn split luciferase system, conditional transgenic V1S/SV2 mice (Figure 1B) were generated to allow cellular resolution of α-syn oligomer formation. In order to analyze expression of S1/S2 and V1S/SV2, mouse brains of 24-month-old mice were dissected in six different brain regions (Figure S1A). For both mouse lines, forebrain areas with olfactory bulb, cortex, and midbrain featured strong expression of human α-syn, whereas hindbrain areas showed moderate to very weak expression levels (Figures 1C and 1D). In V1S/SV2 brains, we detected α-syn dimers/multimers that have been described previously for the split Venus YFP system and were absent in S1/S2 mouse lines (refer to Figure S1B) (Kim et al., 2016; Eckermann et al., 2015; Cai et al., 2018). Conditional transgene expression of S1/S2 as well as V1S/SV2 was confirmed by dox treatment of mice. In both mouse lines, human α-syn protein levels were roughly fourfold higher than endogenous α-syn on western blot (Figure S1C). To further assess α-syn pathology in S1/S2 and V1S/SV2 mice, a phospho-specific antibody was used. Phosphorylated α-syn modification at serine 129 is predominantly found in Lewy bodies and is associated with disease-promoting mechanisms in PD (Oueslati, 2016; Anderson et al., 2006). Extensive p-Ser-129 α-syn signals could be observed in olfactory bulb, cortex, and midbrain in both S1/S2 as well as V1S/SV2 mice (Figures 1C and 1D).

Behavioral analysis of S1/S2 expressing mice showed significant differences compared to dox treated mice in the pole test (two-way repeated-measures ANOVA; $p < 0.001$) (Figures 1E and S1D). Also motor coordination, assessed in the accelerating rotarod (Figure 1F) and beam walking test (Figures 1G and S1E), differed significantly between the two groups (two-way repeated-measures ANOVA; $p < 0.001$). Moreover, hindlimb clasping testing (Figure S1F) demonstrated that S1/S2 expressing mice partially retracted hindlimbs toward the abdomen, starting from 13 months on (two-way repeated-measures ANOVA; $p < 0.001$).

In the open field, α-syn overexpressing mice showed reduced locomotor activity and exploratory behavior (Figures S1G–S1K). In addition, a reduced anxiety-like behavior was observed in the elevated plus maze, as they had the propensity to stay longer in open arms than control animals (Figures S1L and S1M). We addressed V1S/SV2 animal motor behavior by running wheel activity (Figure S1N) and already observed between 8 and 12 months of age a decreased activity for α-syn expressing mice compared to control (two-way repeated-measures ANOVA; $p < 0.001$).

Olfactory dysfunction as an early non-motor symptom in PD (Doty, 2012) was tested in both mouse lines using a buried food test. As illustrated in Figures S1O and S1P, the time to uncover the buried sunflower seeds for S1/S2 mice was significantly longer at 20–24 months of age and V1S/SV2 mice already showed first alterations at 12–16 months of age (two-way repeated-measures ANOVA; $p < 0.001$).

(M) Representative striatal TH staining in V1S/SV2 mice.
(N and O) Striatal TH-immunoreactivity quantification of S1/S2 (N) and V1S/SV2 (O) mice at 5 (n = 5 mice per group) and 24 months of age (n = 6 mice per group). Intensities of tissue sections stained simultaneously were compared. Data: mean ± SEM; paired t test; *$p \leq 0.05$; ns = not significant).
(P) Unsupervised hierarchical clustering of 24-month-old V1S/SV2 transgene expressing (on) and doxycycline treated mice (off), using 10,000 differentially expressed genes. Colors represent overexpression (yellow) or downregulation (blue).
See also Figures S1 and S2 and Tables S1, S2, and S3.

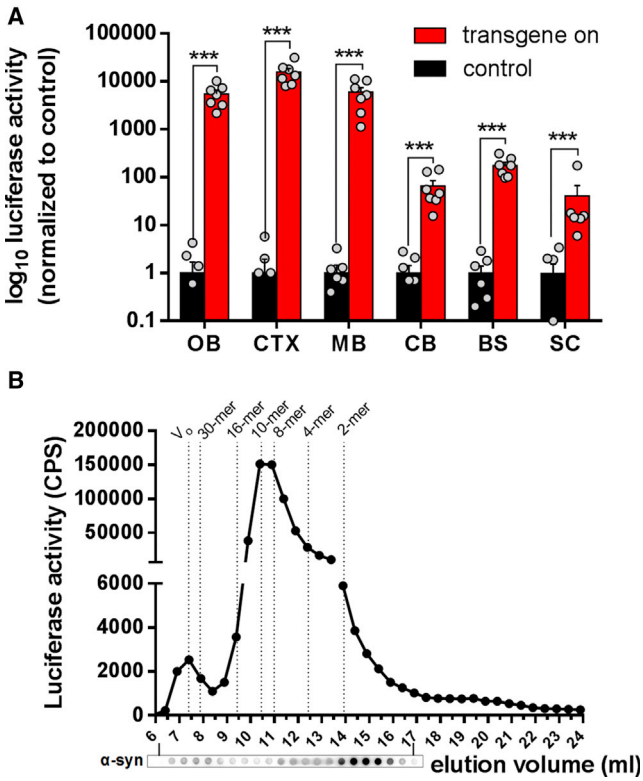

Figure 2. Direct Detection of *De Novo* Generated α-Syn Oligomers *In Vivo* Using the S1/S2 PCA Mouse Model

(A) Normalized Gaussia luciferase activity measurements of S1/S2 brain area lysate. 12–16 months of age (n = 7 mice per group). Brain dissection according to Figure S1A. Data: mean ± SEM, Mann-Whitney *U* test, ***p ≤ 0.001.

(B) Representative luciferase activity of size-exclusion chromatography (SEC) fractions of full-brain lysate of S1/S2 animal (19.5 months of age) and dot blot analysis (anti-human α-syn 15G7 antibody) of SEC fractions (5.9–16.9 ml). Luciferase assay reveals enrichment of 8–16-mer species.

In accordance with these behavioral phenotypes we detected age-dependent alterations of the dopaminergic system in mice expressing S1/S2 or V1S/SV2. In contrast to the pre-symptomatic phase (7 months), a significant reduction of striatal dopamine and elevated levels of striatal dopamine metabolites using high-performance liquid chromatography (HPLC) analysis as well as a reduction of striatal dopaminergic fibers were detected in the striatum at 24 months for both S1/S2 and V1S/SV2 mice (Figures 1H, 1I, 1M, 1N, 1O, and S1Q) whereas serotonin (5-HT) concentrations and the turnover rate were not changed (Figure S1R). Dopamine and 5-HT concentrations in the substantia nigra were not significantly altered for both S1/S2 and V1S/SV2 mice (Figures S1S–S1U). Furthermore, a mild loss of dopaminergic neurons in the substantia nigra using two methods for tyrosine hydroxylase (TH) cell number determination of S1/S2 expressing mice at 24 months of age was observed (Figures 1J and 1K) thus underlining deficits in the dopaminergic system. For 24-month-old V1S/SV2 mice, cell counting of TH-immunopositive neurons reached a significant reduction with method A whereas optical fractionator (method B) did not reach statistical significance (p = 0.166) (Figure 1L).

To also characterize our V1S/SV2 mouse model on a transcriptomic level, sequencing of whole-brain RNA lysates was performed (Figures 1P and S2; Tables S1, S2, and S3). Interestingly, out of 25 relevant significantly altered pathways identified in PD patients versus age-matched healthy controls (Elstner et al., 2011), 22 were also significantly altered in our V1S/SV2 mouse model. Within the highly significant altered mitochondrial dysfunction pathway, we even detected an overlap of individual genes of more than 51% with PD patients, emphasizing the value of these mice as a model for PD.

Detection of an 8–16-mer Oligomeric Subfraction *In Vivo*

To analyze α-syn oligomers *in vivo*, protein complementation in S1/S2 brain extracts was determined using a luciferase assay. Elevated levels of Gaussia luciferase activity indicative for α-syn oligomers were found in olfactory bulb, cortex, and midbrain areas and moderate to low levels in cerebellum, brainstem, and spinal cord (Figure 2A). No luciferase activity could be detected in body fluids (cerebrospinal fluid, whole blood, serum, plasma, or urine) or other organs (gut, stomach, liver, spleen, kidney, heart, or testis).

In contrast to conventional methods, like SDS-PAGE, our approach allowed us to determine the exact sizes of different α-syn species in the brains of S1/S2 mice: Using size-exclusion chromatography (SEC) combined with luciferase activity measurement and dot blot detection of total α-syn in each fraction, we identified a heterogeneous profile of α-syn oligomers. The strongest luciferase signal corresponded to 8–16 mer (in fractions of 10–13 ml) (Figure 2B). Luciferase signals and dot blot (human α-syn specific 15G7 antibody) signals peaked in different fractions (11 and 15 ml, respectively). This suggested that the 8–16-mer α-syn oligomers were highly enriched compared to the total amount of α-syn *in vivo*.

Age-Dependent Accumulation of α-Syn Oligomers

Age is the most prominent risk factor for PD. Therefore, we determined whether age has an impact on α-syn oligomer formation and applied homogenates of different brain areas from 1-, 12-, and 24-month-old S1/S2 mice to SEC with subsequent luciferase activity measurements and dot blot analysis (human α-syn specific 15G7 antibody) of the respective fractions (Figure 3A). We found a dramatic increase in 8–16-meric oligomers in 24-month-old mice compared to 12- and 1-month-old animals. In midbrain (comprising hippocampus [HC], caudoputamen [CP], globus pallidus interna/externa [GPi/e], thalamus, and substantia nigra pars reticulata [SNpr]; see Figure S1A), a considerable number of oligomers larger than 30 mer was formed during aging. In low expressing hindbrain areas (cerebellum, brainstem, and spinal cord), we found a similar pattern with a high percentage of oligomers corresponding to 16 to 4 mers (fractions from 9.5 to 12.5 ml) that were formed with age. Also, quantification of total luciferase activity per brain area (Figure 3B) points to an age-dependent increase of α-syn oligomers. The finding of accumulation of α-syn oligomer species with age led us to categorize the S1/S2 oligomers into subclasses (large, medium, and small oligomers, tetramers, dimers, and α-syn fragments). When we calculated the percentages of the total oligomer count (Figure 3C), we found a stepwise decrease of smaller

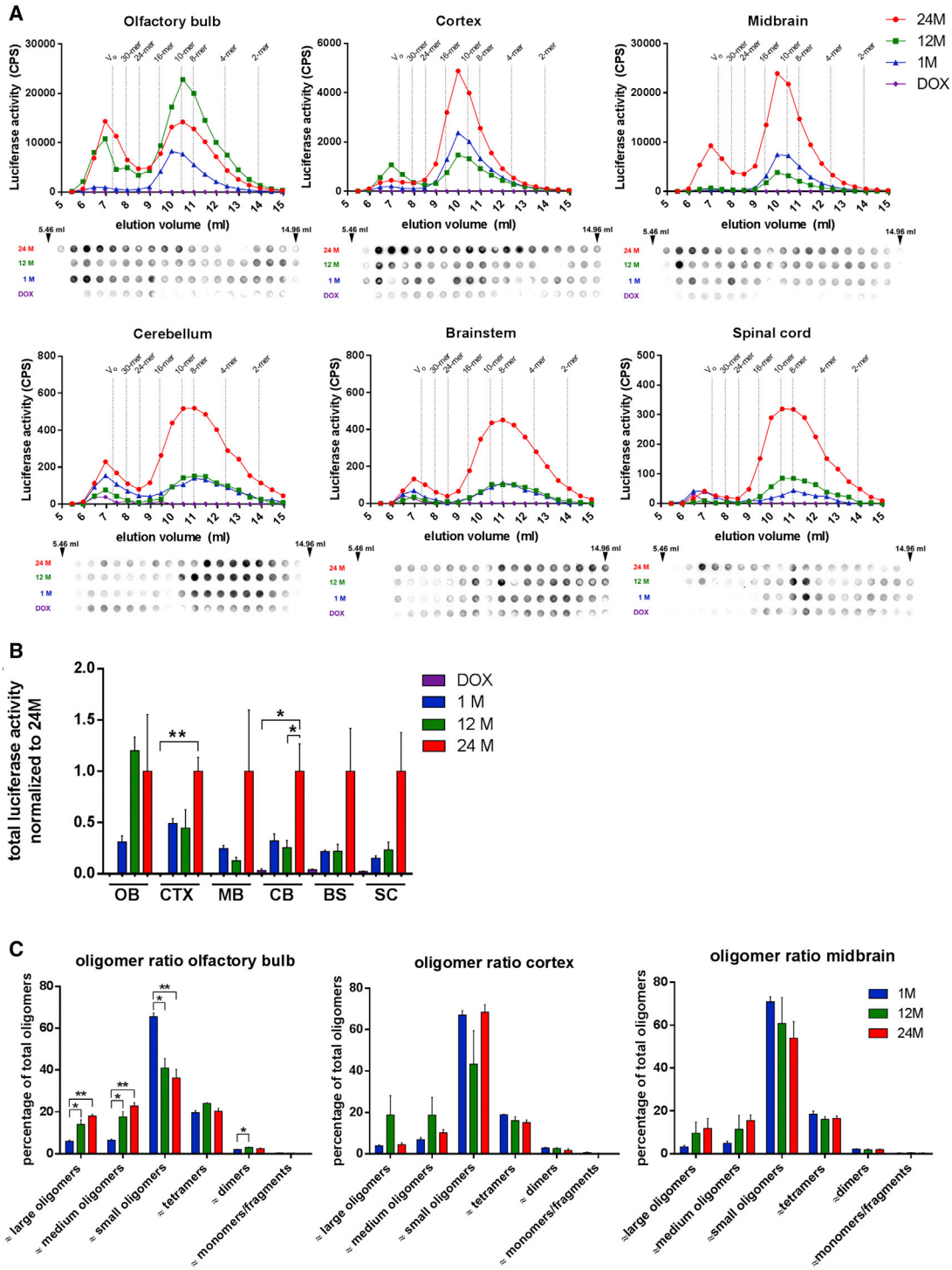

Figure 3. Age-Dependent Increase of 8–16-mer α-Syn Oligomer Species

(A) Luciferase activity measurement of SEC fractions of different brain areas of 1 month (blue), 12 months (green), 24 months (red), and doxycycline treated (purple) S1/S2 mice shows age-dependent accumulation of 8–16-mer oligomer species. Dot blot analysis of respective SEC fractions (5.46–14.96 ml) was performed using anti-human α-syn 15G7 antibody. Graph depicts mean of n = 3 mice per group.

(B) Quantification of total luciferase activity of all SEC fractions per brain area demonstrates an age-dependent increase of α-syn oligomers (area under the curve equivalent; one-way ANOVA with Tukey's post hoc test, *p ≤ 0.05, **p ≤ 0.01; data: mean ± SEM).

(legend continued on next page)

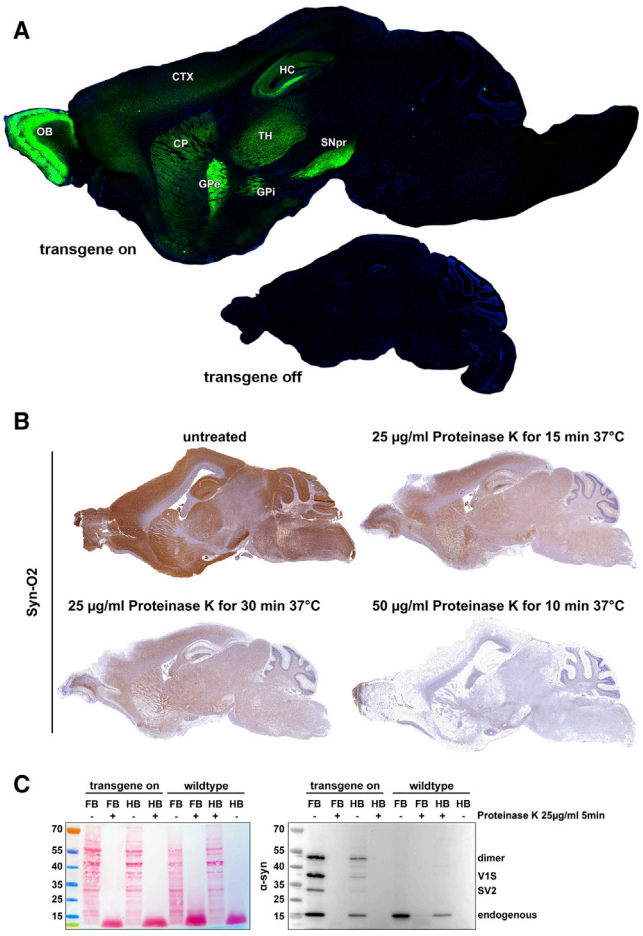

Figure 4. Soluble V1S/SV2 Oligomer Formation in Defined Fore- and Midbrain Areas

(A) Sagittal V1S/SV2 mouse brain sections showing repression of transgene expression by doxycycline (off) and successful complementation of V1S and SV2 in transgene expressing mice (on; green fluorescence) in the olfactory bulb, hippocampus, cortex, caudoputamen, globus pallidus interna/externa, thalamus, and substantia nigra pars reticulata (12-month-old mice; DAPI in blue).

(B) Immunostaining of sagittal V1S/SV2 brain sections (age: 24 months) with anti-aggregated α-syn Syn-O2 antibody and treatment with different Proteinase K conditions demonstrates the solubility of α-syn oligomers.

(C) Western blot (α-syn clone 42 [BD] antibody) and corresponding Ponceau S staining of forebrain (FB) and hindbrain (HB) treated with or without Proteinase K of V1S/SV2 expressing versus wild-type mouse (age: 20 months) showed solubility of V1S/SV2 oligomers. Blots reflect representative result of three independent experiments.

oligomers and simultaneously a stepwise increase of larger oligomers during aging for the olfactory bulb and midbrain. To distinguish whether the age-dependent increase in luciferase activity results from an increase in α-syn protein or from increased generation of α-syn oligomers, densitometry of dot blots using human α-syn antibody was performed. No significant difference in total α-syn between 24-, 12-, and 1-month-old S1/S2 mice could be observed (Figure S3A), indicating an increased α-syn oligomer load with aging.

Subcellular Distribution of α-Syn Oligomers *In Vivo*

Next, we used the V1S/SV2 mouse model for subcellular resolution of α-syn oligomer formation. Reconstituted fluorescent Venus YFP could be detected in defined fore- and midbrain areas, particularly in the olfactory bulb, cortex, hippocampal formation, caudoputamen, globus pallidus, thalamus, and the substantia nigra pars reticulata (Figure 4A), which was abolished by treatment with dox. To also confirm the presence of aggregated α-syn in the V1S/SV2 mouse brain, sections were stained with Syn-O2 antibody, which is specific for aggregated α-syn and stains Lewy bodies and neurites in human tissue (Vaikath et al., 2015). As demonstrated in Figure 4B, immunohistochemistry confirmed the presence of aggregated α-syn species in V1S/SV2 animals. To determine the Proteinase K sensitivity of α-syn aggregates in the brains of 24-month-old V1S/SV2 mice, immunohistochemical analysis was performed in sections after treatment with different Proteinase K conditions. Here, oligomeric α-syn immunoreactivity was considerably reduced, suggesting the presence of Proteinase K soluble α-syn species in V1S/SV2 mice (Figure 4B). Incubation of brain lysate with Proteinase K and subsequent western blot analysis confirmed the soluble nature of V1S/SV2 oligomers in fore- and hindbrain regions (Figure 4C).

To underline the pathophysiological relevance of α-syn oligomers in our mouse model, additional stainings using p-Ser-129 antibody and oligomer-specific Syn-O2 and 5G4 antibodies were performed. Since both oligomeric antibodies Syn-O2 and 5G4 were validated to detect aggregated α-syn in human PD tissue (Kovacs et al., 2012; Vaikath et al., 2015), the high degree of colocalization with V1S/SV2 (84% and 81%, respectively), as well as the strong overlap to p-Ser-129 (77%), underlines the pathological characteristics of formed V1S/SV2 oligomers.

We noticed that Venus YFP reconstitution could be detected solely in fore- and midbrain areas with high synaptic densities and not in the soma or nuclei of neurons. Staining of sagittal brain sections with the presynaptic marker Bassoon revealed the synaptic localization of V1S/SV2 fluorescence (Figure S3B). At large hippocampal mossy fiber synapses, which are 2–5 μm in diameter (Zhao et al., 2012), many α-syn Venus YFP oligomer puncta colocalized with Bassoon signal. In contrast, staining with the postsynaptic marker Homer1 showed a significantly decreased colocalization compared to presynaptic marker Bassoon (Figures 5A and 5B). In addition, the synaptically localized oligomers were mainly composed of human α-syn (15G7 antibody). A partial overlap with endogenous mouse α-syn, as shown by D37A6 antibody staining, also suggests a possible formation of

(C) Percentage of SEC luciferase activity of (A) grouped into α-syn oligomer subclasses shows for OB and MB a stepwise increase of large oligomers and a decrease of smaller oligomers with age. Classification: large oligomers (≤96 mer, >48 mer), medium oligomers (≤38 mer, >15 mer), small oligomers (≤15 mer, >6 mer), tetramers (≤6 mer, ≥3 mer), dimers (<3 mer, >1 mer), and monomers/fragments (≤1 mer). One-way ANOVA with Tukey's post hoc test, *$p \leq 0.05$, **$p \leq 0.01$; data: mean ± SEM.

See also Figure S3.

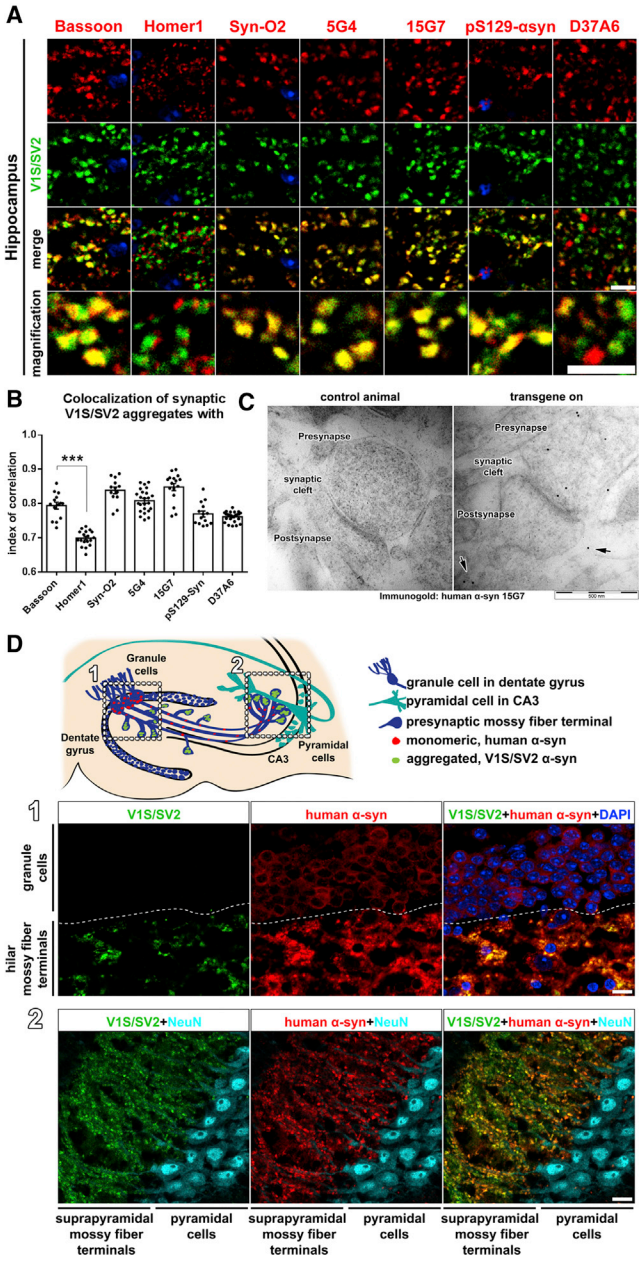

Figure 5. α-Syn Aggregation and Oligomer Formation in the Presynaptic Compartment

(A) Confocal co-staining of V1S/SV2 aggregates in the hilar mossy fiber terminals of the dentate gyrus with presynaptic marker Bassoon, postsynaptic marker Homer1, α-syn aggregate specific Syn-O2 and 5G4 antibodies, human α-syn 15G7 antibody, p-S129- α-syn antibody, and mouse α-syn specific antibody D37A6. Scale bar: 5 μm.

(B) Quantification of (A) using the ImageJ Colocalization Colormap plugin. The index of correlation represents the fraction of positively correlated pixels (n = 13–25 stainings using 3–5 mice; one-way ANOVA with Tukey's post hoc test, ***$p \leq 0.001$; data: mean ± SEM).

(C) Immunogold staining of striatal synapse with anti-human α-syn 15G7 antibody. Representative electron micrographs show the presynaptic localization of α-syn in transgene expressing mice. Potential postsynaptic or extrasynaptic localization of α-syn is indicated with arrows.

heteromers containing both human and mouse α-syn (Figures 5A and 5B). To further characterize the localization of human α-syn, we carried out a post-embedding immunogold labeling of ultrathin sections of the striatum (Figure 5C). Electron micrographs (EMs) confirmed a presynaptic localization of transgenic human α-syn, mainly at the vesicle reserve pool but also close to the active zone of the presynapse. Surprisingly, EM pictures also indicated a potential postsynaptic or extrasynaptic localization of human α-syn (Figure 5C, arrows), which is in agreement with a possible transsynaptic propagation of α-syn.

α-Syn pathology has been described at the synapse (Soukup et al., 2018); however, the site of oligomer formation is still a matter of debate. In V1S/SV2 expressing mice we found phosphorylated Syn-O2 positive V1S/SV2 aggregates solely located at synaptic terminals but not in the cytoplasm of neurons expressing the transgene. We thus hypothesized that α-syn could be present in the cytoplasm, but in an unaggregated state and therefore lacking V1S/SV2 fluorescence. Indeed, immunofluorescent staining clearly demonstrated the presence of cytoplasmic human α-syn in granule cells of the dentate gyrus, which were lacking the V1S/SV2 signal (Figure 5D, 1, upper row). Reconstituted V1S/SV2 fluorescence signal was only observed in mossy fiber terminals in the hilus and at projection terminals to pyramidal neurons in CA3 (Figure 5D, 2, lower row). This indicates that cytoplasmic α-syn is not in an oligomeric state, while the presynapse represents a site for oligomerization that gives rise to pathologically relevant α-syn species *in vivo*.

Cell-to-Cell Transmission of α-Syn

Cell-to-cell transmission of α-syn has been suggested before, but respective experiments were limited to *in vitro* studies, based on injection of exogenously formed α-syn fibrils or transplanted α-syn producing cells (Luk et al., 2012a, 2012b; Rey et al., 2013; Holmqvist et al., 2014; Ulusoy et al., 2013; Desplats et al., 2009; Hansen et al., 2011; Volpicelli-Daley et al., 2011; Danzer et al., 2009, 2007). In contrast, our models offer the chance to assess the propagation of α-syn expressed and formed in host cells *in vivo*.

Assuming a transsynaptic cell-to-cell propagation of α-syn, we postulated the possible existence of cells that were immunopositive for human α-syn protein without the expression the transgenic mRNA (see below; Figure 6E), but with synaptic input from brain areas expressing the transgene. Since the CaMKIIα promoter is primarily limited to glutamatergic forebrain neurons, we searched predominantly in the hindbrain areas for neurons fulfilling these criteria. To avoid autofluorescence artifacts 3,3′-diaminobenzidine (DAB) staining was used for these experiments. Indeed, in the deep cerebellar nuclei (interposed nucleus, fastigial nucleus receiving input from Purkinje layer;

(D-1) Staining for human α-syn (15G7) in the dentate gyrus detects cytoplasmic localization of human α-syn in granule cells that were negative for reconstituted V1S/SV2 signal, indicating that cytoplasmic human α-syn is not aggregated. Scale bar: 10 μm. (D-2) Colocalization of V1S/SV2 (green) and human α-syn antibody staining (15G7, red) in the projection terminals of granule cells to the pyramidal cells of hippocampal CA3 region supports synaptic aggregation and localization. Scale bar: 10 μm.
See also Figure S3.

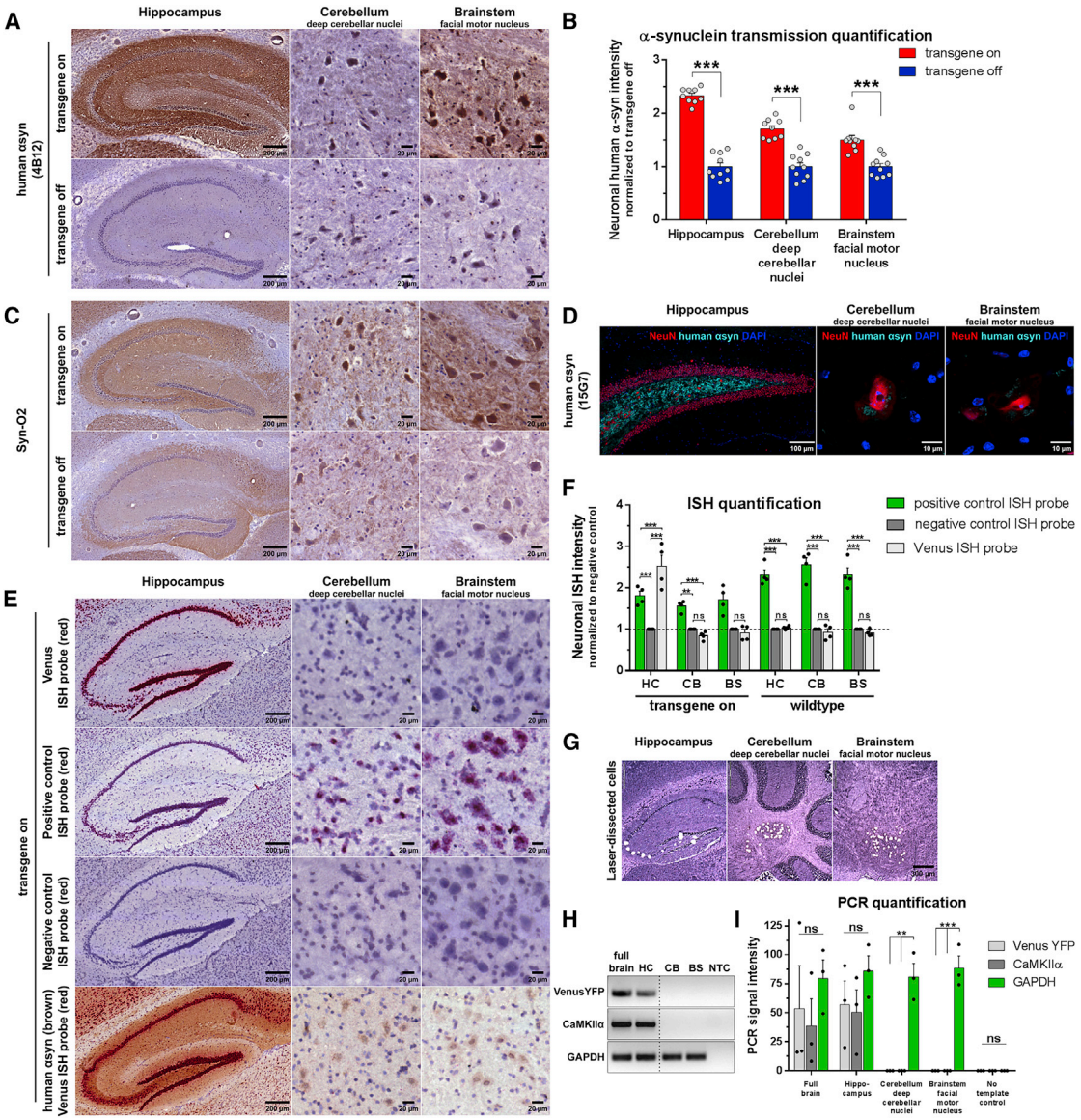

Figure 6. Prion-Like Spreading of α-Syn Aggregates *In Vivo*

(A) Immunostaining for human α-syn (4B12) in sagittal brain sections of adult V1S/SV2 mice ± doxycycline (24 months of age). Although most hindbrain neurons are not expressing CaMKIIα (Mayford et al., 1996b, 1996a), neurons of the deep cerebellar nuclei and facial brainstem nucleus were positively stained for cytoplasmic human α-syn.

(B) Quantification of cytoplasmic human α-syn staining intensity using ImageJ, n(on)=9 stainings/4 mice, n(off)=10 stainings/3 mice. Data: mean of intensities normalized to transgene off ±SEM, 2way ANOVA with Sidak's post hoc test. ***$p \leq 0.001$.

(C) Immunostaining for aggregated α-syn (Syn-O2) in sagittal brain sections of adult V1S/SV2 mice ±doxycycline (24 months of age) highlights oligomeric conformation in CB and BS neurons.

(D) Confocal microscopy showed that punctuate cytoplasmic human αsyn aggregates were located within CB and BS neurons (stained with human αsyn (15G7) and NeuN).

(E) RNAscope *in situ* hybridization of V1S/SV2 sagittal brain section using a custom designed Venus ISH probe, positive control ISH probe and negative control ISH probe. Images are representative results from the same animal stained simultaneously, demonstrating the absence of transgene mRNA in deep cerebellar nuclei and brainstem facial motor nucleus. Bottom panel shows dual staining of Venus mRNA (red, ISH) and human α-syn protein (brown, 4B12 antibody, IHC) on V1S/SV2 tissue section.

(F) Quantification of (E) RNAscope *in situ* hybridization, n=4 mice per group. Data normalized to negative control, 2way ANOVA with Tukey's post hoc test. **$p \leq 0.01$, ***$p \leq 0.001$, ns=not significant; data: mean ±SEM.

(G) Representative image for laser capture microdissected cells used for RT-PCR analysis in (H/I)

(legend continued on next page)

Figure S4A) and in the brainstem-associated facial motor nucleus (receiving cortical input; Figure S4A) we found neurons containing cytoplasmic human α-syn protein (Figures 6A and 6B), suggesting a neuron-to-neuron spreading of α-syn protein. These neurons were also reactive to oligomeric α-syn antibody Syn-O2 (Figure 6C). Additional application of confocal fluorescence microscopy showed that cytoplasmic α-syn aggregates were localized in the perinuclear region (Figure 6D). To exclude the possibility of a potential Venus-tag-dependent effect, we also studied the transmission of α-syn in S1/S2 mice. Quantification of human α-syn in deep cerebellar nuclei and facial motor nucleus also confirmed spreading of α-syn in S1/S2 mice (Figure S4B). In addition, we asked whether endogenous mouse α-syn is transmitted along human α-syn. In hindbrain neurons where we observed transmitted human α-syn (deep cerebellar nuclei and brain stem motor nucleus), endogenous mouse α-syn is expressed. Since this makes it difficult to distinguish between transmitted and expressed mouse α-syn, quantification did not reach statistical significance (Figure S4C). Importantly, we aimed to exclude any leaky promoter activity in the deep cerebellar and in the brainstem-associated facial motor neurons. To that end, we used RNAscope *in situ* hybridization (ISH) for the sensitive detection of Venus YFP mRNA sequences. Brain sections of non-transgenic, WT animals showed reactivity only to the positive control probe but did not react to our Venus YFP target ISH probe, demonstrating its sensitivity (Figures 6F, S5E, S5F, and S5G). In contrast to the anticipated CaMKIIα promoter-driven abundant Venus YFP mRNA expression in hippocampal neurons, deep cerebellar and brainstem facial motor nucleus neurons were clearly negative for Venus mRNA (Figures 6E, 6F, and S5C). To further corroborate that cytoplasmic human α-syn in these neurons is not due to leaky transgene expression but rather a consequence of α-syn protein spread from neuron to neuron, we combined classic immunohistochemistry (IHC) staining against human α-syn with ISH on the same tissue section (Figures 6E, bottom panel, and S5D). Again, we could identify deep cerebellar nuclei and brainstem facial motor nucleus neurons positive for human α-syn but negative for transgene mRNA on the same tissue section. However, transmission of transgenic α-syn is not only restricted to hindbrain areas, since we also observed in thalamic areas intracellular accumulations of human α-syn in neurons that did not express the transgene mRNA (Figure S6).

To further exclude a leaky transgene expression in the previously mentioned hindbrain neurons by an alternative method, we applied laser capture microdissection (LCM) followed by DNase treatment and RT-PCR. Quantification of CaMKIIα with exon-exon spanning primers was additionally used as an indirect readout for transgene expression, since Venus YFP transgene lacks introns. We found that only in full-brain RNA lysate and hippocampal RNA were robust amounts of CaMKIIα and Venus YFP mRNA detected, whereas deep cerebellar nuclei neurons (cerebellum [CB]) and facial motor nucleus neurons (brainstem [BS]) were devoid of Venus YFP and CaMKIIα mRNA (Figures 6G–6I). We thereby provided additional evidence to exclude that leaky expression of α-syn in hindbrain neurons is the reason for the α-syn content in these neurons and corroborated the hypothesis of neuron-to-neuron spreading from Venus-YFP-α-syn expressing forebrain neurons to hindbrain neurons.

Since we observed a dopamine deficiency in aged mice, we asked if human α-syn oligomers were present in the cytoplasm of SNpc neurons. Confocal fluorescence microscopy clearly demonstrated intracellular α-syn aggregates (Figures 7A, arrowheads, and 7B) in TH-positive neurons in transgene expressing animals that were absent when transgene expression was turned off. Intriguingly, we did not detect Venus transgene mRNA (red, ISH staining; asterisks) in TH-positive neurons of the SNpc (brown, IHC TH staining; arrows) (Figure 7B). Instead, only smaller, TH-negative neurons in the SNpc had detectable Venus transgene mRNA (Lacey et al., 1989; Nedergaard and Greenfield, 1992). Because the red ISH staining can be difficult to distinguish from brown IHC (TH immunostaining), we took advantage of the fluorescent properties of the red Venus probe dye to separate the signals but still did not detect any dopaminergic neurons expressing the Venus transgene mRNA. A plausible explanation for this finding is that *de novo* generated human α-syn oligomers can spread from transgene expressing glutamatergic afferents of the SNpc to dopaminergic SNpc neurons.

DISCUSSION

We present two transgenic mouse models that allow for directly assessing the quantity and subcellular distribution of α-syn oligomers *in vivo*. Using these mice, we demonstrate an age-dependent accumulation of α-syn oligomers of a defined size and can directly track their localization to the synaptic site *in vivo*. Furthermore, we provide *in vivo* evidence for cell-to-cell transfer of α-syn oligomers from forebrain to hindbrain neurons, without injection of proteins into the tissue or using allogeneic transplanted cells.

Although great effort has been expended to characterize α-syn oligomers in *in vitro* and also *in vivo* models using biochemical methods like SDS-PAGE, the full picture of α-syn oligomer characteristics *in vivo* is still not clear. While SDS-PAGE or antibody-based techniques reflect only a subset of α-syn oligomers, our approach using size-exclusion chromatography combined with luciferase measurements unveils the existence of the whole range of different α-syn oligomers in various brain regions *in vivo*. Our animal models not only prove generation of different α-syn oligomers *de novo in vivo,* but also identify an enrichment of a 12-mer oligomeric α-syn. This accumulation of 12 mer was specifically enhanced with age, while the total amount of α-syn protein was not increased in old animals. This age-dependent alteration in the α-syn oligomer profile was

(H) RT-PCR analysis of laser capture microdissected cells using primers for V1S transgene, CaMKIIα as an indirect readout for promoter activity and GAPDH. Full brain RNA lysate of V1S/SV2 mice served as positive control. NTC=no template control. One lane was removed (dotted line).
(I) Quantification of PCR result of laser capture microdissected cells in (G/I) using ImageJ, n=3, 2way ANOVA with Tukey's post hoc test. $^{**}p \leq 0.01$, $^{***}p \leq 0.001$, ns=not significant; data: mean ±SEM.
See also Figures S4, S5, S6, and S7.

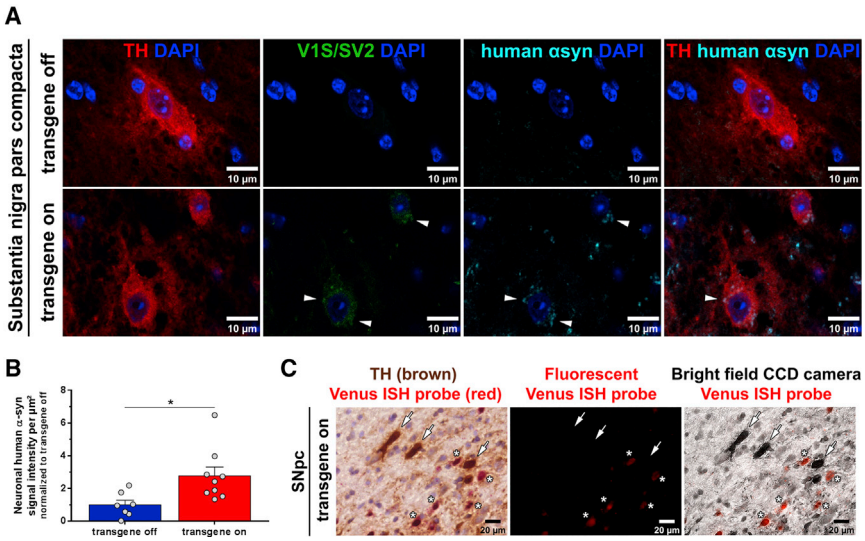

Figure 7. Transmission of Human α-syn to Dopaminergic Neurons in the SNpc

(A) Confocal fluorescent co-staining of TH (red) and human α-syn (cyan, 15G7) together with V1S/SV2 (green) showed presence of cytoplasmic α-syn aggregates in dopaminergic neurons of the SNpc (arrowheads) of V1S/SV2 expressing mice.

(B) Quantification of human α-syn in dopaminergic neurons (n(on) = 9 stainings/3 mice, n(off) = 7 stainings/2 mice, data normalized to transgene off and presented as mean ± SEM; two-tailed unpaired t test, *p ≤ 0.05).

(C) (Left panel) Dopaminergic neurons of the SNpc (arrows) do not express the transgene (asterisks) as demonstrated by dual staining of Venus ISH probe targeting transgene mRNA (red) and TH protein (brown) in V1S/SV2 mice, indicating a spread of α-syn protein to dopaminergic neurons.

paralleled by a late onset, progressive motor decline, and a loss of dopaminergic neurons in S1/S2 mice.

Our study cannot provide a final proof for a causative link between α-syn oligomers, TH cell numbers, and/or behavioral alterations. Nevertheless, our data are in line with the study of Nuber et al. (2008), who also used a CaMKIIα-driven conditional α-syn mouse model and reported that even a small nominal change in dopaminergic neurons might account for a clinical phenotype. For 24-month-old S1/S2 mice, we observed a reduced anxiety-like behavior that is similar to a previously described transgenic α-syn mouse model (George et al., 2008). Reduced striatal dopamine levels have recently been reported to cause less anxiety (Wenzel et al., 2018), which directly links the observed phenotype in S1/S2 mice to a lack of dopamine. However, the question remains whether monomeric or oligomeric α-syn provokes dopamine depletion in our model. Since the overall amount of human α-syn remained constant over time but the oligomeric profile changed in S1/S2 mice, we hypothesize that the oligomeric species interferes with synaptic signaling and dopamine homeostasis.

Our RNA sequencing (RNA-seq) approach revealed a remarkable similarity with RNA-seq data from laser captured dopaminergic SNpc neurons of PD patients (Elstner et al., 2011). Cellular processes in the aged human brain, along with increased levels of α-syn during aging in nigral neurons (Chu and Kordower, 2007), might also lead to a massive increase in α-syn oligomers in humans. Aging is the most prominent risk factor for the development of PD (Baldereschi et al., 2000; de Lau and Breteler, 2006; Collier et al., 2011). Therefore, a higher oligomeric load of α-syn during aging might be an explanation for a higher vulnerability for PD upon aging.

Strong evidence indicates that synaptic pathology is central in PD (Calo et al., 2016). In patients with dementia with Lewy bodies many α-syn aggregates are located at the synapse, leading to synaptic impairment and neurodegeneration (Kramer and Schulz-Schaeffer, 2007). Moreover, α-syn accumulation at presynaptic terminals affects neurotransmitter release and redistribution of presynaptic proteins in an age-dependent manner (Burré, 2015; Kramer and Schulz-Schaeffer, 2007; Garcia-Reitböck et al., 2010; Busch et al., 2014), even prior to the death of dopaminergic neurons (Bridi and Hirth, 2018). While it has been speculated that α-syn accumulation in presynaptic terminals causes synaptopathy with subsequent "dying back" of neurons, we were able to demonstrate that α-syn oligomerization takes place at the presynapse and not in the α-syn protein containing cytoplasm *in vivo*. This finding also suggests an aggregation-promoting environment in the presynaptic compartment. The result that most V1S/SV2 aggregates were recognized by oligomer-specific antibodies such as Syn-O2 and 5G4, which bind also to human α-syn oligomers, further suggest that V1S/SV2 oligomers share important properties with pathological forms of α-syn in humans. We demonstrated the presence of Ser129-phosphorylated α-syn oligomers at the presynapse *in vivo*, consistent with previous data detecting p-Ser129-α-syn-positive aggregates at the presynapse in dementia with Lewy bodies patients (Colom-Cadena et al., 2017). Together, this identifies the synapse as a pathophysiologically relevant cellular compartment in PD. However, it remains an interesting question whether α-syn aggregates are formed at synapses to fulfill a physiological function, as suggested by Wang et al. (2014), whether they have detrimental effects, or both. A reorganization of α-syn into multimers at synapses has also been observed before using V1S/SV2 transfected hippocampal neurons (Wang et al., 2014).

However, the detection of V1S/SV2 oligomers mainly at presynaptic terminals in both our V1S/SV2 mouse model and the study by Wang et al. is in contrast to two other studies (Dimant et al., 2013; Cai et al., 2018). In this case, α-syn oligomers were detected in cell bodies of neurons, as detected by a Venus YFP fluorescence complementation system. This discrepancy can be plausibly explained by the use of adeno-associated viral vectors to target overexpression of V1S/SV2 to the soma of nigral neurons under the control of a highly active chicken β-actin promoter in both studies (Dimant et al., 2013; Cai et al., 2018). In contrast, moderate V1S/SV2 expression was achieved in our mouse model by the CaMKIIα promoter, or by a molecular replacement strategy achieving endogenous levels of α-syn in the study by Wang et al. (2014).

Aggregated and oligomeric α-syn are also implicated in prion-like transmission of PD pathology between distant axonally connected brain regions (Jucker and Walker, 2013). According to the hypothesis by Braak et al. (2003), spread of α-syn pathology follows connected brain areas. Consistent with this hypothesis, we detected cytoplasmic human α-syn accumulation in neurons of the deep cerebellar nuclei and in neurons of the brainstem facial motor nucleus despite the absence of transgenic mRNA, as shown by *in situ* hybridization and RT-PCR of laser capture microdissected cells.

These neurons receive afferent projections from distant neurons expressing the transgene, which is in agreement with a possible transsynaptic spread of α-syn (Figure S7). In addition, electron microscopy of human α-syn immunogold labeled striatal sections depicted extra-neuronal α-syn, which would be consistent with a neuron-to-neuron transmission. Furthermore, although the CaMKIIα promoter is active in glutamatergic but not dopaminergic neurons (Liu and Murray, 2012), we found dopaminergic neurons that harbored human α-syn aggregates. This provides a further argument for spreading of α-syn from transgene expressing glutamatergic neurons to dopaminergic neurons in the substantia nigra.

In summary, we have generated two non-invasive inducible transgenic mouse models that allow the direct quantification and subcellular visualization of α-syn oligomers *in vivo*. Employing these *in vivo* tools, we demonstrate an age-dependent increase of distinct α-syn oligomer species, their presence at the synapse, and ultimately the spread of α-syn oligomers to distant, axonally connected neuronal populations *in vivo*.

STAR★METHODS

Detailed methods are provided in the online version of this paper and include the following:

SUPPLEMENTAL INFORMATION

Supplemental Information can be found online at https://doi.org/10.1016/j.celrep.2019.10.089.

ACKNOWLEDGMENTS

We thank T. Christ, R. Bueck, and A. Jesionek for excellent work. We thank F. Roselli for ISH assistance. We also thank the Core Facility for transgenic animals and for Laser Microscopy at Ulm University. Moreover, we are grateful to R. Marienfeld from CCCU for the opportunity to work with the Zeiss PALM MicroBeam system. This work was supported by the Deutsche Forschungsgemeinschaft (DFG) Emmy Noether Research Group DA 1657/2-1 and GRK 1789 (CEMMA), funds from the Junior Professorship Program Baden-Wuerttemberg, as well as FWF SFB F-44 and DFG LI-1745/1.

AUTHOR CONTRIBUTIONS

M.K. and K.M.D. designed the project. O.S., B.v.E., and B.B. established transgenic mouse lines. M.K. performed experiments and analyzed the data. S.L. and A.B.E. performed RNA-seq analysis. M.K. and V.G. analyzed the results with IPA. L.H., B.H.F., R.P., and B.L. performed stereology of TH neurons, and R.P. supported vibratome sectioning. P.V. and B.F. performed HPLC analysis. D.M. assisted with SEC assays. D.W. helped with mouse experiments. B.M. performed statistical analysis. V.G., P.W., B.B., A.C.L., P.J.M., and J.H.W. provided intellectual input. M.K., J.H.W., and K.M.D. wrote the manuscript. All authors reviewed and approved the manuscript.

DECLARATION OF INTERESTS

The authors declare no competing interests.

Received: October 2, 2018
Revised: September 16, 2019
Accepted: October 22, 2019
Published: November 26, 2019

SUPPORTING CITATIONS

The following reference appears in the Supplemental Information: Lalonde and Strazielle, 2011.

REFERENCES

Aelvoet, S.A., Ibrahimi, A., Macchi, F., Gijsbers, R., Van den Haute, C., Debyser, Z., and Baekelandt, V. (2014). Noninvasive bioluminescence imaging of α-synuclein oligomerization in mouse brain using split firefly luciferase reporters. J. Neurosci. *34*, 16518–16532.

Anderson, J.P., Walker, D.E., Goldstein, J.M., de Laat, R., Banducci, K., Caccavello, R.J., Barbour, R., Huang, J., Kling, K., Lee, M., et al. (2006). Phosphorylation of Ser-129 is the dominant pathological modification of alpha-synuclein in familial and sporadic Lewy body disease. J. Biol. Chem. *281*, 29739–29752.

Auluck, P.K., Caraveo, G., and Lindquist, S. (2010). α-Synuclein: membrane interactions and toxicity in Parkinson's disease. Annu. Rev. Cell Dev. Biol. *26*, 211–233.

Baldereschi, M., Di Carlo, A., Rocca, W.A., Vanni, P., Maggi, S., Perissinotto, E., Grigoletto, F., Amaducci, L., and Inzitari, D.; ILSA Working Group. Italian Longitudinal Study on Aging (2000). Parkinson's disease and parkinsonism in a longitudinal study: two-fold higher incidence in men. Neurology *55*, 1358–1363.

Bankhead, P., Loughrey, M.B., Fernández, J.A., Dombrowski, Y., McArt, D.G., Dunne, P.D., McQuaid, S., Gray, R.T., Murray, L.J., Coleman, H.G., et al. (2017). QuPath: Open source software for digital pathology image analysis. Sci. Rep. *7*, 16878.

Barrett, P.J., and Timothy Greenamyre, J. (2015). Post-translational modification of α-synuclein in Parkinson's disease. Brain Res. *1628* (*Pt B*), 247–253.

Braak, H., Del Tredici, K., Rüb, U., de Vos, R.A., Jansen Steur, E.N., and Braak, E. (2003). Staging of brain pathology related to sporadic Parkinson's disease. Neurobiol. Aging *24*, 197–211.

Bridi, J.C., and Hirth, F. (2018). Mechanisms of α-Synuclein Induced Synaptopathy in Parkinson's Disease. Front. Neurosci. *12*, 80.

Burré, J. (2015). The Synaptic Function of α-Synuclein. J. Parkinsons Dis. *5*, 699–713.

Busch, D.J., Oliphint, P.A., Walsh, R.B., Banks, S.M., Woods, W.S., George, J.M., and Morgan, J.R. (2014). Acute increase of α-synuclein inhibits synaptic vesicle recycling evoked during intense stimulation. Mol. Biol. Cell *25*, 3926–3941.

Cai, W., Feng, D., Schwarzschild, M.A., McLean, P.J., and Chen, X. (2018). Bimolecular Fluorescence Complementation of Alpha-synuclein Demonstrates its Oligomerization with Dopaminergic Phenotype in Mice. EBioMedicine *29*, 13–22.

Calo, L., Wegrzynowicz, M., Santivañez-Perez, J., and Grazia Spillantini, M. (2016). Synaptic failure and α-synuclein. Mov. Disord. *31*, 169–177.

Carter, R.J., Morton, J., and Dunnett, S.B. (2001). Motor coordination and balance in rodents. Curr. Protoc. Neurosci. *Chapter 8*, Unit 8.12.

Chu, Y., and Kordower, J.H. (2007). Age-associated increases of alpha-synuclein in monkeys and humans are associated with nigrostriatal dopamine depletion: Is this the target for Parkinson's disease? Neurobiol. Dis. *25*, 134–149.

Collier, T.J., Kanaan, N.M., and Kordower, J.H. (2011). Ageing as a primary risk factor for Parkinson's disease: evidence from studies of non-human primates. Nat. Rev. Neurosci. *12*, 359–366.

Colom-Cadena, M., Pegueroles, J., Herrmann, A.G., Henstridge, C.M., Muñoz, L., Querol-Vilaseca, M., Martín-Paniello, C.S., Luque-Cabecerans, J., Clarimon, J., Belbin, O., et al. (2017). Synaptic phosphorylated α-synuclein in dementia with Lewy bodies. Brain *140*, 3204–3214.

Danzer, K.M., Haasen, D., Karow, A.R., Moussaud, S., Habeck, M., Giese, A., Kretzschmar, H., Hengerer, B., and Kostka, M. (2007). Different species of alpha-synuclein oligomers induce calcium influx and seeding. J. Neurosci. *27*, 9220–9232.

Danzer, K.M., Krebs, S.K., Wolff, M., Birk, G., and Hengerer, B. (2009). Seeding induced by alpha-synuclein oligomers provides evidence for spreading of alpha-synuclein pathology. J. Neurochem. *111*, 192–203.

Danzer, K.M., Ruf, W.P., Putcha, P., Joyner, D., Hashimoto, T., Glabe, C., Hyman, B.T., and McLean, P.J. (2011). Heat-shock protein 70 modulates toxic extracellular α-synuclein oligomers and rescues trans-synaptic toxicity. FASEB J. *25*, 326–336.

de Lau, L.M., and Breteler, M.M. (2006). Epidemiology of Parkinson's disease. Lancet Neurol. *5*, 525–535.

Dehay, B., Bourdenx, M., Gorry, P., Przedborski, S., Vila, M., Hunot, S., Singleton, A., Olanow, C.W., Merchant, K.M., Bezard, E., et al. (2015). Targeting α-synuclein for treatment of Parkinson's disease: mechanistic and therapeutic considerations. Lancet Neurol. *14*, 855–866.

Delenclos, M., Trendafilova, T., Jones, D.R., Moussaud, S., Baine, A.M., Yue, M., Hirst, W.D., and McLean, P.J. (2016). A Rapid, Semi-Quantitative Assay to Screen for Modulators of Alpha-Synuclein Oligomerization Ex vivo. Front. Neurosci. *9*, 511.

Desplats, P., Lee, H.J., Bae, E.J., Patrick, C., Rockenstein, E., Crews, L., Spencer, B., Masliah, E., and Lee, S.J. (2009). Inclusion formation and neuronal cell death through neuron-to-neuron transmission of alpha-synuclein. Proc. Natl. Acad. Sci. USA *106*, 13010–13015.

Dimant, H., Kalia, S.K., Kalia, L.V., Zhu, L.N., Kibuuka, L., Ebrahimi-Fakhari, D., McFarland, N.R., Fan, Z., Hyman, B.T., and McLean, P.J. (2013). Direct detection of alpha synuclein oligomers in vivo. Acta Neuropathol. Commun. *1*, 6.

Doty, R.L. (2012). Olfactory dysfunction in Parkinson disease. Nat. Rev. Neurol. *8*, 329–339.

Eckermann, K., Kügler, S., and Bähr, M. (2015). Dimerization propensities of Synucleins are not predictive for Synuclein aggregation. Biochim. Biophys. Acta *1852*, 1658–1664.

Elstner, M., Morris, C.M., Heim, K., Bender, A., Mehta, D., Jaros, E., Klopstock, T., Meitinger, T., Turnbull, D.M., and Prokisch, H. (2011). Expression analysis of dopaminergic neurons in Parkinson's disease and aging links transcriptional dysregulation of energy metabolism to cell death. Acta Neuropathol. *122*, 75–86.

Fujiwara, H., Hasegawa, M., Dohmae, N., Kawashima, A., Masliah, E., Goldberg, M.S., Shen, J., Takio, K., and Iwatsubo, T. (2002). alpha-Synuclein is phosphorylated in synucleinopathy lesions. Nat. Cell Biol. *4*, 160–164.

Fusco, G., Chen, S.W., Williamson, P.T.F., Cascella, R., Perni, M., Jarvis, J.A., Cecchi, C., Vendruscolo, M., Chiti, F., Cremades, N., et al. (2017). Structural basis of membrane disruption and cellular toxicity by α-synuclein oligomers. Science *358*, 1440–1443.

Garcia-Reitböck, P., Anichtchik, O., Bellucci, A., Iovino, M., Ballini, C., Fineberg, E., Ghetti, B., Della Corte, L., Spano, P., Tofaris, G.K., et al. (2010). SNARE protein redistribution and synaptic failure in a transgenic mouse model of Parkinson's disease. Brain *133*, 2032–2044.

George, S., van den Buuse, M., San Mok, S., Masters, C.L., Li, Q.X., and Culvenor, J.G. (2008). Alpha-synuclein transgenic mice exhibit reduced anxiety-like behaviour. Exp. Neurol. *210*, 788–792.

Gossen, M., and Bujard, H. (1992). Tight control of gene expression in mammalian cells by tetracycline-responsive promoters. Proc. Natl. Acad. Sci. USA *89*, 5547–5551.

Guyenet, S.J., Furrer, S.A., Damian, V.M., Baughan, T.D., La Spada, A.R., and Garden, G.A. (2010). A simple composite phenotype scoring system for evaluating mouse models of cerebellar ataxia. J. Vis. Exp. (*39*), 1787.

Hansen, C., Angot, E., Bergström, A.L., Steiner, J.A., Pieri, L., Paul, G., Outeiro, T.F., Melki, R., Kallunki, P., Fog, K., et al. (2011). α-Synuclein propagates from mouse brain to grafted dopaminergic neurons and seeds aggregation in cultured human cells. J. Clin. Invest. *121*, 715–725.

Hodara, R., Norris, E.H., Giasson, B.I., Mishizen-Eberz, A.J., Lynch, D.R., Lee, V.M., and Ischiropoulos, H. (2004). Functional consequences of alpha-synuclein tyrosine nitration: diminished binding to lipid vesicles and increased fibril formation. J. Biol. Chem. *279*, 47746–47753.

Holmqvist, S., Chutna, O., Bousset, L., Aldrin-Kirk, P., Li, W., Björklund, T., Wang, Z.Y., Roybon, L., Melki, R., and Li, J.Y. (2014). Direct evidence of Parkinson pathology spread from the gastrointestinal tract to the brain in rats. Acta Neuropathol. *128*, 805–820.

Jucker, M., and Walker, L.C. (2013). Self-propagation of pathogenic protein aggregates in neurodegenerative diseases. Nature *501*, 45–51.

Kim, D.K., Lim, H.S., Kawasaki, I., Shim, Y.H., Vaikath, N.N., El-Agnaf, O.M., Lee, H.J., and Lee, S.J. (2016). Anti-aging treatments slow propagation of synucleinopathy by restoring lysosomal function. Autophagy *12*, 1849–1863.

Kovacs, G.G., Wagner, U., Dumont, B., Pikkarainen, M., Osman, A.A., Streichenberger, N., Leisser, I., Verchère, J., Baron, T., Alafuzoff, I., et al. (2012). An antibody with high reactivity for disease-associated α-synuclein reveals extensive brain pathology. Acta Neuropathol. *124*, 37–50.

Kramer, M.L., and Schulz-Schaeffer, W.J. (2007). Presynaptic alpha-synuclein aggregates, not Lewy bodies, cause neurodegeneration in dementia with Lewy bodies. J. Neurosci. *27*, 1405–1410.

Lacey, M.G., Mercuri, N.B., and North, R.A. (1989). Two cell types in rat substantia nigra zona compacta distinguished by membrane properties and the actions of dopamine and opioids. J. Neurosci. *9*, 1233–1241.

Lalonde, R., and Strazielle, C. (2011). Brain regions and genes affecting limb-clasping responses. Brain Res. Brain Res. Rev. *67*, 252–259.

Liu, X.B., and Murray, K.D. (2012). Neuronal excitability and calcium/calmodulin-dependent protein kinase type II: location, location, location. Epilepsia *53*, 45–52.

Luk, K.C., Kehm, V., Carroll, J., Zhang, B., O'Brien, P., Trojanowski, J.Q., and Lee, V.M. (2012a). Pathological α-synuclein transmission initiates Parkinson-like neurodegeneration in nontransgenic mice. Science *338*, 949–953.

Luk, K.C., Kehm, V.M., Zhang, B., O'Brien, P., Trojanowski, J.Q., and Lee, V.M. (2012b). Intracerebral inoculation of pathological α-synuclein initiates a rapidly progressive neurodegenerative α-synucleinopathy in mice. J. Exp. Med. *209*, 975–986.

Mayford, M., Bach, M.E., Huang, Y.Y., Wang, L., Hawkins, R.D., and Kandel, E.R. (1996a). Control of memory formation through regulated expression of a CaMKII transgene. Science *274*, 1678–1683.

Mayford, M., Baranes, D., Podsypanina, K., and Kandel, E.R. (1996b). The 3′-untranslated region of CaMKII alpha is a cis-acting signal for the localization and translation of mRNA in dendrites. Proc. Natl. Acad. Sci. USA *93*, 13250–13255.

Nedergaard, S., and Greenfield, S.A. (1992). Sub-populations of pars compacta neurons in the substantia nigra: the significance of qualitatively and quantitatively distinct conductances. Neuroscience *48*, 423–437.

Nuber, S., Petrasch-Parwez, E., Winner, B., Winkler, J., von Hörsten, S., Schmidt, T., Boy, J., Kuhn, M., Nguyen, H.P., Teismann, P., et al. (2008). Neurodegeneration and motor dysfunction in a conditional model of Parkinson's disease. J. Neurosci. *28*, 2471–2484.

Oueslati, A. (2016). Implication of Alpha-Synuclein Phosphorylation at S129 in Synucleinopathies: What Have We Learned in the Last Decade? J. Parkinsons Dis. *6*, 39–51.

Outeiro, T.F., Putcha, P., Tetzlaff, J.E., Spoelgen, R., Koker, M., Carvalho, F., Hyman, B.T., and McLean, P.J. (2008). Formation of toxic oligomeric alpha-synuclein species in living cells. PLoS ONE *3*, e1867.

Paleologou, K.E., Oueslati, A., Shakked, G., Rospigliosi, C.C., Kim, H.Y., Lamberto, G.R., Fernandez, C.O., Schmid, A., Chegini, F., Gai, W.P., et al. (2010). Phosphorylation at S87 is enhanced in synucleinopathies, inhibits alpha-synuclein oligomerization, and influences synuclein-membrane interactions. J. Neurosci. *30*, 3184–3198.

Putcha, P., Danzer, K.M., Kranich, L.R., Scott, A., Silinski, M., Mabbett, S., Hicks, C.D., Veal, J.M., Steed, P.M., Hyman, B.T., and McLean, P.J. (2010). Brain-permeable small-molecule inhibitors of Hsp90 prevent alpha-synuclein oligomer formation and rescue alpha-synuclein-induced toxicity. J. Pharmacol. Exp. Ther. *332*, 849–857.

Rey, N.L., Petit, G.H., Bousset, L., Melki, R., and Brundin, P. (2013). Transfer of human α-synuclein from the olfactory bulb to interconnected brain regions in mice. Acta Neuropathol. *126*, 555–573.

Rosborough, K., Patel, N., and Kalia, L.V. (2017). α-Synuclein and Parkinsonism: Updates and Future Perspectives. Curr. Neurol. Neurosci. Rep. *17*, 31.

Soukup, S.F., Vanhauwaert, R., and Verstreken, P. (2018). Parkinson's disease: convergence on synaptic homeostasis. EMBO J. *37*, e98960.

Sung, J.Y., Park, S.M., Lee, C.H., Um, J.W., Lee, H.J., Kim, J., Oh, Y.J., Lee, S.T., Paik, S.R., and Chung, K.C. (2005). Proteolytic cleavage of extracellular secreted alpha-synuclein via matrix metalloproteinases. J. Biol. Chem. *280*, 25216–25224.

Ulusoy, A., Rusconi, R., Pérez-Revuelta, B.I., Musgrove, R.E., Helwig, M., Winzen-Reichert, B., and Di Monte, D.A. (2013). Caudo-rostral brain spreading of α-synuclein through vagal connections. EMBO Mol. Med. *5*, 1119–1127.

Vaikath, N.N., Majbour, N.K., Paleologou, K.E., Ardah, M.T., van Dam, E., van de Berg, W.D., Forrest, S.L., Parkkinen, L., Gai, W.P., Hattori, N., et al. (2015). Generation and characterization of novel conformation-specific monoclonal antibodies for α-synuclein pathology. Neurobiol. Dis. *79*, 81–99.

Volpicelli-Daley, L.A., Luk, K.C., Patel, T.P., Tanik, S.A., Riddle, D.M., Stieber, A., Meaney, D.F., Trojanowski, J.Q., and Lee, V.M. (2011). Exogenous α-synuclein fibrils induce Lewy body pathology leading to synaptic dysfunction and neuron death. Neuron *72*, 57–71.

Wang, L., Das, U., Scott, D.A., Tang, Y., McLean, P.J., and Roy, S. (2014). α-synuclein multimers cluster synaptic vesicles and attenuate recycling. Curr. Biol. *24*, 2319–2326.

Wenzel, J.M., Oleson, E.B., Gove, W.N., Cole, A.B., Gyawali, U., Dantrassy, H.M., Bluett, R.J., Dryanovski, D.I., Stuber, G.D., Deisseroth, et al. (2018). Phasic Dopamine Signals in the Nucleus Accumbens that Cause Active Avoidance Require Endocannabinoid Mobilization in the Midbrain. Curr. Biol. *28*, 1392–1404.e5.

Winner, B., Jappelli, R., Maji, S.K., Desplats, P.A., Boyer, L., Aigner, S., Hetzer, C., Loher, T., Vilar, M., Campioni, S., et al. (2011). In vivo demonstration that alpha-synuclein oligomers are toxic. Proc. Natl. Acad. Sci. USA *108*, 4194–4199.

Yang, M., and Crawley, J.N. (2009). Simple behavioral assessment of mouse olfaction. Curr. Protoc. Neurosci. *Chapter 8*, Unit 8.24.

Zhao, S., Studer, D., Chai, X., Graber, W., Brose, N., Nestel, S., Young, C., Rodriguez, E.P., Saetzler, K., and Frotscher, M. (2012). Structural plasticity of spines at giant mossy fiber synapses. Front. Neural Circuits *6*, 103.

STAR★METHODS

KEY RESOURCES TABLE

REAGENT or RESOURCE	SOURCE	IDENTIFIER
Antibodies		
Mouse monoclonal anti-Bassoon; 1:200	Enzo, Farmingdale, NY, USA	Clone SAP7F407 Cat# ADI-VAM-PS003-D; RRID:AB_2038857
Polyclonal rabbit anti-Homer1; 1:200	Synaptic Systems, Goettingen, Germany	Cat# 160 002; RRID:AB_2120990
Rabbit monoclonal anti-NeuN; 1:400	Abcam, Cambridge, UK	Clone EPR12763; RRID:AB_2532109
Rabbit polyclonal anti-Tyrosine Hydroxylase; 1:200/400	Merck, Darmstadt, Germany	Cat# AB152; RRID:AB_390204
Mouse monoclonal anti-Phosphorylated α-Synuclein; 1:500/1:1000	Wako, Osaka, Japan	Clone pSyn #64; RRID:AB_2537218
Rat monoclonal anti-α-Synuclein (human specific); 1:100	Enzo, Farmingdale, NY, USA	Clone 15G7 Cat# ALX-804-258-L001; RRID:AB_2050691
Mouse monoclonal anti-α-Synuclein (human specific); 1:100	BioLegend, San Diego, CA, USA	Clone 4B12; RRID:AB_2734561
Rabbit monoclonal anti-α-Synuclein XP (mouse specific); 1:200	Cell Signaling Technology, Cambridge, UK	Clone D37A6 Cat# 4179S; RRID:AB_1904156
Mouse monoclonal anti-α-Synuclein (aggregated); 1:100	BioLegend, San Diego, CA, USA	Clone Syn-O2 Cat# 847602; RRID:AB_2632701
Mouse monoclonal anti-α-Synuclein (aggregated); 1:600	Merck, Darmstadt, Germany	Clone 5G4 Cat# MABN389; RRID:AB_2716647
Mouse monoclonal anti-α-Synuclein; 1:1000	BD, Franklin Lakes, NJ, USA	Clone 42 Cat# 610786; RRID:AB_398107
Rabbit polyclonal anti-GAPDH; 1:2500	Proteintech, Rosemont, IL, USA	Cat# 10494-1-AP; RRID:AB_2263076
Rabbit monoclonal anti-GFP N-term; 1:1000	Cell Signaling Technology, Cambridge, UK	Clone D5.1 Cat# 2956; RRID:AB_1196615
Goat anti-Rabbit IgG (H+L) Cross-Adsorbed Secondary Antibody, HRP	Thermo Fisher Scientific, Waltham, MA, USA	Cat# G-21234; RRID:AB_2536530
Goat anti-Mouse IgG (H+L) Cross-Adsorbed Secondary Antibody, HRP	Thermo Fisher Scientific, Waltham, MA, USA	Cat# G-21040; RRID:AB_2536527
Goat anti-Rat IgG (H+L) Cross-Adsorbed Secondary Antibody, Alexa Fluor 546	Thermo Fisher Scientific, Waltham, MA, USA	Cat# A-11081; RRID:AB_2534125
Goat anti-Rabbit IgG (H+L) Cross-Adsorbed Secondary Antibody, Alexa Fluor 546	Thermo Fisher Scientific, Waltham, MA, USA	Cat# A-11010; RRID:AB_2534077
Goat anti-Mouse IgG (H+L) Cross-Adsorbed Secondary Antibody, Alexa Fluor 546	Thermo Fisher Scientific, Waltham, MA, USA	Cat# A-11003; RRID:AB_2534071

(*Continued on next page*)

Continued

REAGENT or RESOURCE	SOURCE	IDENTIFIER
Goat anti-Rat IgG (H+L)		Cat# A-21247; RRID:AB_141778
Cross-Adsorbed	Thermo Fisher	
Secondary Antibody,	Scientific, Waltham,	
Alexa Fluor 647	MA, USA	
Goat anti-Rabbit IgG		Cat# A-21244; RRID:AB_2535812
(H+L) Cross-Adsorbed	Thermo Fisher	
Secondary Antibody,	Scientific, Waltham,	
Alexa Fluor 647	MA, USA	
Goat anti-Mouse IgG		Cat# A-21235; RRID:AB_2535804
(H+L) Cross-Adsorbed	Thermo Fisher	
Secondary Antibody,	Scientific, Waltham,	
Alexa Fluor 647	MA, USA	
Goat-anti-Rat IgG (H+L)		Cat# 810.455; RRID:N/A
cross adsorbed against	Aurion,	
Mouse immunoglobulins,	Wageningen,	
10 nm gold labeled	Netherlands	
	Jackson	Cat# 715-007-003; RRID:AB_2307338
AffiniPure Fab Fragment	ImmunoResearch,	
Donkey Anti-Mouse IgG	West Grove, PA,	
(H+L)	USA	
Chemicals, Peptides, and Recombinant Proteins		
Coelenterazine	PJK GmbH, Kleinblittersdorf, Germany	Cat# 102171
Doxycycline hyclate	AppliChem GmbH, Darmstadt, Germany	Cat# A2951
Critical Commercial Assays		
QuickExtract DNA Extraction Solution	Lucigen Corporation, Middleton, WI, USA	Cat# QE09050
miRNeasy Mini Kit	QIAGEN, Venlo, Netherlands	Cat# 217004
PicoPure RNA Isolation Kit	Thermo Fisher Scientific, Waltham, MA, USA	Cat# KIT0204
iScript cDNA Synthesis Kit	Bio-Rad Laboratories, Inc., Hercules, CA, USA	Cat# 1708891
Pierce BCA Protein Assay Kit	Thermo Fisher Scientific, Waltham, MA, USA	Cat# 23225
RNase-Free DNase Set	QIAGEN, Venlo, Netherlands	Cat# 79254
RNAscope 2.5 HD Detection Reagent – RED	ACD, Newark, CA, USA	Cat# 322350/322360
Gel Filtration Calibration Kit	GE Healthcare, Chicago, IL, USA	Cat# 28403841
Liquid DAB+ Substrate Chromogen System	Dako/Agilent, Santa Clara, CA, USA	Cat# K3468
Deposited Data		
RNA sequencing data of 24 months old V1S/SV2 mice	This paper	GEO: GSE134462
Experimental Models: Mouse		
B6-Tg(ind alpha-syn split Luci)D; Camk2a-tTA	This paper	N/A
B6-Tg(ind alpha-syn split Venus)D; Camk2a-tTA	This paper	N/A
Oligonucleotides		
Genotyping: tTA_For: 5′-CGC TGT GGG GCA TTT TAC TTT AG-3′	This paper	N/A
Genotyping: tTA_Rev: 5′-CAT GTC CAG ATC GAA ATC GTC-3′	This paper	N/A

(*Continued on next page*)

Continued

REAGENT or RESOURCE	SOURCE	IDENTIFIER
Genotyping: S1/S2_For: 5′-CAC CGA GAA CAA CGA AGA CTT-3′	This paper	N/A
Genotyping: S1/S2_Rev: 5′-CGT CCT GGG ATG AAC TTC TT-3′	This paper	N/A
Genotyping: V1S/SV2_For: 5′-ACA TGA AGC AGC ACG ACT TCT-3′	This paper	N/A
Genotyping: V1S/SV2_Rev: 5′-ACG TTG TGG CTG TTG TAG TTG TA-3′	This paper	N/A
PCR: Venus_For: 5′-GAC GAC GGC AAC TAC AAG AC-3′	This paper	N/A
PCR: Venus_Rev: 5′-CCA CCA TCG ATC TGC TTG TC-3′	This paper	N/A
PCR: CaMKIIα_For: 5′-CAG CAT CCC AGC CCT AGT TC-3′	This paper	N/A
PCR: CaMKIIα_Rev: 5′-CCC CAC CAG TAA CCA GAT CG-3′	This paper	N/A
PCR: GAPDH_For: 5′-AGT ATG ACT CCA CTC ACG GCA A-3′	This paper	N/A
PCR: GAPDH_Rev: 5′-ATA CTC AGC ACC GGC CTC ACC-3′	This paper	N/A
RNAscope® Probe- YFP-synSNCA	This paper/ACD, Newark, CA, USA	Cat# 514241
Software and Algorithms		
GraphPad Prism Version 6.01	GraphPad Software, Inc., San Diego, CA, USA	https://www.graphpad.com
SAS 9.4	SAS Institute GmbH, Heidelberg, Germany	https://www.sas.com
ImageJ 1.52a	National Institutes of Health, Bethesda, MD, USA	https://imagej.nih.gov/ij
QuPath open source software 0.1.2	Queen's University Belfast, UK	https://qupath.github.io
Viewer 2 tracking software	Biobserve GmbH, Bonn, Germany	http://www.biobserve.com/behavioral research
Maus Vital software	Laser- und Medizin-Technologie Berlin, Berlin, Germany	N/A
Zen 2.3	Zeiss, Oberkochen, Germany	https://www.zeiss.de/corporate/home.html
LAS AF Lite 4.3	Leica Biosystems, Wetzlar, Germany	https://www.leicabiosystems.com
iTEM software	Olympus Soft Imaging Solutions GmbH, Münster, Germany	https://www.olympus-sis.com
Adobe Photoshop 12.0	Adobe Inc., San José, CA, USA	https://www.adobe.com
StereoInvestigator 7.5	MBF Bioscience, Williston, VT, USA	https://www.mbfbioscience.com
Chromeleon 6.5 HPLC software	Dionex GmbH, Idstein, Germany	https://www.thermofisher.com/us/en/home
FastQC	Babraham Bioinformatics, Babraham Institute, UK	https://www.bioinformatics.babraham.ac.uk/projects/fastqc
Cutadapt	Marcel Martin	http://journal.embnet.org/index.php/embnetjournal/article/view/200
fqtrim	Center for Computational Biology, Johns Hopkins University, MD, USA	https://ccb.jhu.edu/software/fqtrim
SAMtools 1.3.1.	Heng Li	http://www.htslib.org
STAR	Cold Spring Harbor Laboratory, NY, USA	10.1093/bioinformatics/bts635
Subread 1.5.3	Walter+Eliza Hall, Institute of Medical Research, Melbourne, Australia	http://subread.sourceforge.net
DESeq2	Michael Love, Simon Anders, Wolfgang Huber	https://bioconductor.org/packages/DESeq2

(*Continued on next page*)

Continued

REAGENT or RESOURCE	SOURCE	IDENTIFIER
biomaRt	Steffen Durinck, Wolfgang Huber, Sean Davis, Francois Pepin, Vince S Buffalo, Mike Smith	https://bioconductor.org/packages/biomaRt
Ingenuity Pathway Analysis	QIAGENbioinformatics	https://www.qiagenbioinformatics.com

LEAD CONTACT AND MATERIALS AVAILABILITY

Further information and requests for resources, reagents, and mice should be directed to and will be fulfilled by the Lead Contact Karin Danzer (karin.danzer@uni-ulm.de). Transfer of materials may require a material transfer agreement (MTA) to be signed.

EXPERIMENTAL MODEL AND SUBJECT DETAILS

Ethical Statement

Mouse experiments were performed in accordance with provisions of the German Animal Welfare Act (Tierschutzgesetz) and in line with the local guidelines of the Animal Research Center, Ulm University.

Generation of Transgenic Animals

Constructs for S1, S2 and V1S, SV2 (described previously in Danzer et al., 2011) were cloned into multiple cloning sites of the pBI5 bidirectional vector downstream of the tetracycline response element (TRE). Vectors were linearized with BsrBI, DNA fragments were purified from agarose gel with UltraClean 15 DNA Purification Kit (MO BIO, Carlsbad, CA, US) and 2 ng/μl were injected into the pronucleus of fertilized oocytes. Transgenic founder lines were crossbred with mice expressing the tetracycline transactivator (tTA) under control of the Calcium/calmodulin-dependent protein kinase II α (CaMKIIα) promoter B6.Cg-Tg(Camk2a-tTA)1Mmay/DboJ obtained from Jackson Laboratory. Transgenic offspring were genotyped by PCR of tail DNA using the following oligonucleotides for TRE sequence. S1/S2 animals: S1/S2_For: 5′-CAC CGA GAA CAA CGA AGA CTT-3′; S1/S2_Rev: 5′-CGT CCT GGG ATG AAC TTC TT-3′. V1S/SV2 animals: V1S/SV2_For: 5′-ACA TGA AGC AGC ACG ACT TCT-3′; V1S/SV2_Rev: 5′-ACG TTG TGG CTG TTG TAG TTG TA-3′. For tTA sequence: tTA_For: 5′-CGC TGT GGG GCA TTT TAC TTT AG-3′; tTA_Rev: 5′-CAT GTC CAG ATC GAA ATC GTC-3′.

Housing and Gender of Mice Used in the Analyses

Animals were housed at the Animal Research Center, Ulm University under standardized conditions (SPF) with food/water *ad libitum* and a 14/10 h light/dark cycle. Transgene expression was turned off with 100 mg/l doxycycline in the drinking water, sweetened with 10 g/l glucose. For transgene expression, animals were given water supplemented with 10 g/l glucose after weaning.

Male mice were used for behavioral tests, RNA-seq, TH stereology, TH striatal density measurements, western blot analysis, immunohistochemistry, and *in situ* hybridization. Female mice were used for electron microscopy. Balanced mixed sex groups were used for HPLC dopamine concentration analysis, size-exclusion chromatography, and luciferase activity assays.

Protein Complementation Assay

For S1/S2 line, Gaussia luciferase is split in two parts and each part is fused to human wild-type α-syn. Both parts, S1 and S2, are expressed simultaneously. For V1S/SV2 line, the fluorescent protein VenusYFP is split and each non-fluorescent part is fused to α-syn (V1S and SV2). Upon α-syn oligomerization, the reporter parts form a functional reconstituted bioluminescent active luciferase (S1/S2) or a fluorescent VenusYFP protein (V1S/SV2). In both lines, transgene expression is designed in a Tet-off system inducible manner, driven by the neuronal specific CaMKIIα promoter (Mayford et al., 1996a). Application of doxycycline ceases transgene expression (Figures 1A and 1B).

METHOD DETAILS

RNA Isolation for RNA Sequencing

RNA isolation was performed using the miRNeasy Mini Kit (QIAGEN, Venlo, Netherlands) following manufacturer's instructions with initial 700 μl Qiazol / 50 mg tissue and DNase digestion. RNA sequencing was carried out by Next-Generation-Sequencing Core Unit Erlangen. The quality of reads was assessed using FastQC. Adaptor sequences and stretches with low quality were then removed using cutadapt with the settings -a AGATCGGAAGAGC -q 20,20–minimum-length 50–trim-n–max-n = 0.1, followed by another round of FastQC. Reads mapping to tRNA or rRNA sequences (obtained from RepBase, mapped with bwa) were discarded. Following another filtering step with fqtrim, reads were mapped to the reference genome using STAR. ENSEMBL GRCm38 (UCSC mm10) served as reference genome and version 85 of the ENSEMBL annotation set for mm10 was used. Indexing of the aligned .bam files was done using samtools 1.3.1. Expression matrices were then generated using the featureCounts routine of subread 1.5.3. Differential expression calls were obtained from DESeq2 with standard settings. The resulting expression matrices were annotated using

the mm10 annotation set from the biomaRt package. Gene regulation pathways were generated with Ingenuity Pathway Analysis (QIAGENbioinformatics). The complete RNA sequencing dataset has been uploaded to GEO, the accession number is: GEO: GSE134462.

Western Blot

Mouse brain samples were dissected according to Figure S1A and homogenized in RIPA buffer (ratio 1 g tissue per 10 mL buffer, measured with analytical balance) (150 mM NaCl, 1% NP-40, 0.5% sodium deoxycholate, 0.1% SDS buffer, 50 mM Tris, pH 8.0) for 2 × 2 min at 25 Hz using a TissueLyser II (QIAGEN, Venlo, Netherlands). Samples were centrifuged at 1.000 g for 5 min, 4°C. Supernatant was normalized to equal protein amount by BCA assay (Thermo Fisher Scientific, Waltham, MA, USA), followed by ultracentrifugation for 1 h, 4°C at 100.000 g (soluble fraction). 40 μg protein samples were separated on NuPAGE 4%–12% Bis-Tris gels by using a XCell SureLock Mini-Cell Electrophoresis system and transferred to a PVDF membrane, using a XCell SureLock XCell II Blot Module (Thermo Fisher Scientific, Waltham, MA, USA). Specific antigens were detected with the following primary antibodies: mouse anti-α-syn clone 42 (BD, Franklin Lakes, NJ, USA), mouse anti-phosphorylated α-syn clone pSyn#64 (Wako, Osaka, Japan) and rabbit anti-GAPDH 10494-1-AP (Proteintech, Rosemont, IL, USA). HRP-conjugated goat secondary antibodies were supplied from Promega. Images were acquired on a FUSION SOLO S (Vilber, Eberhardzell, Germany) with Luminata Forte HRP substrate (Merck, Darmstadt, Germany).

Human Gaussia Luciferase Assay

Dissected brain parts were homogenized in Opti-MEM (Thermo Fisher Scientific, Waltham, MA, USA) using a TissueLyser II (QIAGEN, Venlo, Netherlands) for 2 × 2 min at 25 Hz. Samples were centrifuged at 20.800 g for 15 min, 4°C. 0.5 mg protein in 100 μl (duplicates) were used for luciferase activity measurement in an automated plate reader (Victor X3 microplate reader, Perkin-Elmer, Waltham, USA) with automated injection of the cell permeable substrate coelenterazine (40 μM, P.J.K., Kleinblittersdorf, Germany) and signal integration time of 1 s.

Size-Exclusion Chromatography (SEC)

Mouse brain samples were dissected according to Figure S1A and homogenized in PBS (1 g tissue per 15 mL PBS, measured with analytical balance) using a TissueLyser II (2 × 2 min at 25 Hz). Samples were centrifuged at 20.800 g for 30 min, 4°C and 600 μl supernatant were loaded onto a PBS equilibrated 24 mL Superdex 200 (10/300 GL) column (GE Healthcare, Chicago, IL, USA) connected to an ÄKTApurifier (GE Healthcare, Chicago, IL, USA). The protein eluate was monitored by UV absorbance at 280 and 215 nm (flow rate 0.75 ml/min) and fractions of 500 μl were collected for luciferase activity measurement (100 μl, duplicates) and dot blot analysis (100 μl). Molecular mass of protein eluate was estimated using the Gel Filtration Calibration Kit (GE Healthcare, Chicago, IL, USA) with the following standard proteins: Ferritin (440 kDa), Aldolase (158 kDa), Conalbumin (75 kDa), Ovalbumin (44 kDa), Carbonic anhydrase (29 kDa), Ribonuclease A (13.7 kDa) and protinin A (6.5 kDa).

Dot Blot

100 μl of SEC fractions were analyzed using a Dot blot apparatus (Whatman Schleicher & Schuell Minifold I Spot-Blot system, GE Healthcare, Chicago, IL, USA). Briefly, samples were applied on a nitrocellulose membrane (Amersham Protran 0.2, GE Healthcare, Chicago, IL, USA) and the liquid was filtered through the membrane by gentle vacuum. Specific antigens were detected with rat anti-human α-syn 15G7 antibody (Enzo, Farmingdale, NY, USA, 1:100). HRP-conjugated goat secondary antibodies were supplied from Promega. Images were acquired on a FUSION SOLO S (Vilber, Eberhardzell, Germany) with Luminata Forte HRP substrate (Merck, Darmstadt, Germany). Densitometry of SEC fractions (5.46–14.96 ml) was performed using ImageJ (NIH).

Histology

Mice were deeply anaesthetized with ketamine (WDT, Garbsen, Germany)/xylazine (Bayer, Leverkusen, Germany) and transcardially perfused with PBS. Brains were dissected, incubated overnight at 4°C in 30% sucrose, embedded in Tissue-Tek® O.C.T (Sakura, Leiden, Netherlands) and immediately frozen on dry ice and stored at −80°C. Unfixed 12 μm cryostat sections were cut using a Leica CM1850 and mounted on Superfrost Plus slides (Thermo Fisher Scientific, Waltham, MA, USA).

For fluorescent stainings, mouse brain sections were fixed in 2% PFA for 30 min, washed with PBS and permeabilized with 0.5% Saponin + 0.3% Triton X-100. After washing with PBS, tissue sections were blocked with ImmunoBlock (Carl Roth, Karlsruhe, Germany) for 1 h at room temperature (RT). If the primary antibody was raised in mouse, AffiniPure Fab Fragment Donkey Anti-Mouse IgG (H+L) (Jackson ImmunoResearch, West Grove, PA, USA) was added to the blocking solution. Primary antibodies were incubated for 1.5 h at RT and washed for 30 min with PBS. Secondary antibodies coupled to fluorescent dyes (Alexa Fluor 546, 647) were diluted 1:750 and incubated for 1 h at RT. After washing for 30 min with PBS, sections were mounted with DAPI Fluoromount-G (Southern biotech, Birmingham, AL, USA). Fluorescent images were recorded using a confocal LSM710 microscope (Zeiss, Oberkochen, Germany).

For DAB staining, sections were fixed with 4% PFA, treated with 3% H_2O_2 for 30 min at RT after permeabilization step and primary antibody was incubated overnight at 4°C. HRP-conjugated goat secondary antibodies (Thermo Fisher Scientific, Waltham, MA, USA) were diluted 1:200. Sections were incubated with diaminobenzidine (DAB) using Liquid DAB+ Substrate Chromogen System (Dako/Agilent, Santa Clara, CA, USA) according to manufacturer's instructions and counterstained in Mayer's hemalum (Merck, Darmstadt,

Germany) solution for 5 s. After blueing, sections were dehydrated in ascending ethanol series, incubated in Xylol and mounted with DPX (Sigma-Aldrich, St. Louis, MO, USA). Images were recorded using a MIRAX Desk slide scanner (Zeiss, Oberkochen, Germany).

The following primary antibodies were used for histology:

Target	clone/ identifier	Dilution	Company
Bassoon; ms	SAP7F407	1:200	Enzo, Farmingdale, NY, USA
Homer1; rb	160 002	1:200	Synaptic Systems, Goettingen, Germany
NeuN; rb	EPR12763	1:400	Abcam, Cambridge, UK
Tyrosine Hydroxylase; rb	AB152	1:200/400	Merck, Darmstadt, Germany
Phosphorylated α-Synuclein; ms	pSyn #64	1:500	Wako, Osaka, Japan
α-Synuclein (human specific); rat	15G7	1:100	Enzo, Farmingdale, NY, USA
α-Synuclein (human specific); ms	4B12	1:100	BioLegend, San Diego, CA, USA
α-Synuclein (mouse specific); rb	D37A6	1:200	Cell Signaling Technology, Cambridge, UK
α-Synuclein, aggregated; ms	Syn-O2	1:100	BioLegend, San Diego, CA, USA
α-Synuclein, aggregated; ms	5G4	1:600	Merck, Darmstadt, Germany

Electron Microscopy and Immunogold Labeling

Mice were deeply anaesthetized with ketamine (WDT, Garbsen, Germany)/xylazine (Bayer, Leverkusen, Germany) and transcardially perfused with PBS and 4% PFA. Brains were dissected and 150 μm vibratome sections were used to punch out striatal areas. After high-pressure freezing, samples were freeze-substituted with 0.06% uranyl acetate and 5% H_2O in acetone, washed with −20°C propanol and embedded in LR-gold resin. Ultrathin sections (80 nm) were blocked with ImmunoBlock (Carl Roth, Karlsruhe, Germany) for 10 min and primary antibody anti-human α-Synuclein (15G7, rat, dilution 1:5; Enzo, Farmingdale, NY, USA) was incubated for 30 min. Samples were washed in blocking solution 6x2 min and treated with 10 nm gold labeled secondary antibody goat anti-rat IgG (1:50, cross-adsorbed with mouse; Aurion, Wageningen, Netherlands) for 30 min. After washing in blocking solution for 3x2 min and PBS 3x2 min, samples were fixed in 1% glutaraldehyde, washed 4x2 min in ddH_2O, contrasted with 1% uranyl acetate and washed in ddH_2O. Images of ultrathin immunogold labeled sections were recorded using a JEM-1400 transmission electron microscope (Jeol, Akishima, Japan) equipped with a Veleta digital camera (Olympus Soft Imaging Solutions GmbH, Münster, Germany) and iTEM software (Olympus Soft Imaging Solutions GmbH, Münster, Germany).

Proteinase K Treatment

Sagittal 12 μm mouse brain sections were incubated with 25 or 50 μg/ml Proteinase K (Thermo Fisher Scientific, Waltham, MA, USA) in 10 mM Tris HCl pH 7.8; 100 mM NaCl; 0.2% SDS for 15 and 30 min at 37°C, followed by staining procedure as described previously.

Brain lysates of 24 months old V1S/SV2 mice or wild-type controls were incubated with 25 μg/ml Proteinase K for 5 min, followed by Western blot procedure as described above.

RNAscope® *In Situ* Hybridization (ISH)

Mice were anaesthetized with ketamine (WDT, Garbsen, Germany)/xylazine (Bayer, Leverkusen, Germany), transcardially perfused with PBS, brains were dissected, embedded in Tissue-Tek® O.C.T (Sakura, Leiden, Netherlands), immediately frozen on dry ice and stored at −80°C for a short period of time (up to 4 weeks). Sagittal 12 μm mouse brain sections were cut on a cryostat and slides were temporary stored at −80°C. *In situ* hybridization was carried out with RNAscope 2.5 HD Detection Reagent – RED (ACD, Newark, CA, USA) and was performed according to manufacturer's instructions for fresh frozen tissue. Positive control probe targeting mRNA of PPIB housekeeping gene, negative control probe binding to mRNA of bacterial dapB gene as well as custom designed specific target probe for VenusYFP N terminus were purchased from ACD. For dual ISH + IHC staining, RNAscope standard protocols were applied. Primary antibody concentrations: mouse anti-α-Synuclein 4B12 (Biolegend, San Diego, CA, USA) 1:50; rabbit anti-Tyrosine Hydroxylase AB152 (Merck, Darmstadt, Germany) 1:200. HRP-conjugated goat secondary antibodies (Thermo Fisher Scientific, Waltham, MA, USA) were used at 1:250.

Laser Capture Microdissection

Briefly, sagittal mouse brain cryostat sections (12 μm) were placed on UV light pre-treated PEN membrane slides, washed in PBS for 5 min, stained with Mayer's hemalum solution (Merck, Darmstadt, Germany) and dehydrated in ascending ethanol series and stored at −80°C overnight. Laser capture microdissection was performed using a PALM MicroBeam system (Zeiss, Oberkochen, Germany). Cells were collected in PCR tubes (AdhesiveCap 200 opaque, Zeiss, Oberkochen, Germany) and stored for a short time at −80°C (up to 1 week). RNA isolation was performed using the PicoPure RNA Isolation Kit (Thermo Fisher Scientific, Waltham, MA, USA) with DNase treatment. cDNA synthesis was carried out with iScript cDNA Synthesis Kit (Bio-Rad) with subsequent PCR using the

following primers: Venus_For: 5′-GAC GAC GGC AAC TAC AAG AC-3′, Venus_Rev: 5′-CCA CCA TCG ATC TGC TTG TC-3′; CaMKIIα_For: 5′-CAG CAT CCC AGC CCT AGT TC-3′, CaMKIIα_Rev: 5′-CCC CAC CAG TAA CCA GAT CG-3′; GAPDH_For: 5′-AGT ATG ACT CCA CTC ACG GCA A-3′, GAPDH_Rev: 5′-ATA CTC AGC ACC GGC CTC ACC-3′. PCR was verified by agarose gel electrophoresis.

Electrophoresis

2% agarose gels (1.6 g agarose in 80 mL 1x TAE buffer (40 mM Tris, 20 mM acetic acid, 1 mM EDTA, pH 8) + 4 μl of 0.0025% ethidium bromide solution) were used in this study. Samples were mixed with 6x DNA Gel Loading Dye (Thermo Fisher Scientific, Waltham, MA, USA) and GeneRuler 100 bp Plus DNA ladder (Thermo Fisher Scientific, Waltham, MA, USA) was applied for sizing of samples. Electrophoresis was performed at 120 V for up to 1 h.

Behavioral Experiments

Animals were housed in groups in a Scantainer with controlled room temperature, humidity, a 12 h dark/light cycle and food/water *ad libitum*. Cages were enriched with polycarbonate houses and nesting material. For all experiments, 15 male mice per group were tested biweekly (unless stated otherwise) from 3 months on to 24 months. S1/S2 mice underwent the following tests: Pole test analysis, accelerating rotarod, beam walk analysis, hindlimb clasping, buried food test, open field analysis and elevated plus-maze. Since V1S/SV2 mice were housed at a different facility they underwent only a basic characterization by running wheel activity analysis and buried food test. Experiments were carried out at the same time of day. Experimenters conducting all behavioral experiments were blinded to genotype and treatment.

For ***Pole test analysis***, animals were placed head upward on a vertical dowel rod (diameter: 1 cm; height: 65 cm) with five cable ties on top (1 cm distance in between) for better grip and time to orientate downward (TTurn) as well as total time on the pole were recorded (TTotal). Pole test was performed in five consecutive trials and mean values were used for evaluation.

Accelerating rotarod (five lane rotarod, Med Associates) was adjusted to increase from 4 to 40 rpm over a period of 300 s and was carried out in three consecutive trials with 5 min break in between. The latency to fall was recorded and mean values were used for analysis.

The ***beam walk analysis*** setup was constructed as depicted in Carter et al. (2001). Time to cross the round wooden beam (diameter: 11 mm) as well as number of hindlimb foot slips were recorded.

We assessed ***hindlimb clasping*** response and scoring according to Guyenet et al. (2010). Animals were grasped at the base of the tail, lifted for 10 s and hindlimb position was observed. Score of 0 means hindlimbs were constantly splayed outward. For score of 1, one hindlimb was retracted toward the abdomen for more than 5 s. For both hindlimbs retracted toward the abdomen for more than 5 s, the animal received a score of 2. Total retraction of both hindlimbs and contact to the abdomen for more than 5 s resulted in a score of 3. The test was performed at distinct time points with 3 consecutive trials with 5 min break intervals. Average values were used for analysis.

To address a potential reduced olfaction in our animals, we performed a ***buried food test*** according to Yang and Crawley (2009), using sunflower seeds (Seeberger, Ulm, Germany) as palatable food. Briefly, animals were fasted over night for 12 h but fed two consecutive days before with four sunflower seeds for odor familiarization. On the test day, S1/S2 animals were placed in a clean test cage with new bedding, acclimated for 5 min and were transferred temporarily to a transition cage when four sunflower seeds were buried together 3 cm underneath the bedding in alternating corners of the test cage. The animals were reintroduced to the test cage and latency to uncover the seeds was recorded. The recording time was stopped when animals scored the max. value of 300 s searching. V1S/SV2 animals, housed individually due to running wheel activity, were tested in their home cage.

Running wheel activity was monitored (V1S/SV2 animals) with ''Maus Vital'' software (Laser- und Medizin-Technologie Berlin, Berlin, Germany). Mice were housed separately with free access to running wheels from 5 months to 24 months of age. Only full wheel rotations were monitored and recorded every night automatically for 12 hours. A threshold of 1500 revolutions per night was defined for data analysis in order to eliminate obstructed running wheels or passive animals.

Open field as a test for initial locomotion and activity of S1/S2 mice was performed for 10 min in a 50 × 50 cm illuminated arena, border zone was defined as area 8 cm from the wall, center zone area was determined as 16% of total arena (20 x 20 cm). Mice were placed in the center zone and recorded from above. Data were analyzed by Viewer 2 tracking software (Biobserve GmbH, Bonn, Germany).

S1/S2 mice anxiety-related behavior was investigated using the ***elevated plus-maze***, raised 60 cm off the floor. The maze had two open and two closed arms with similar lengths (wall height of closed arms: 16 cm), connected by a central platform of 5 × 5 cm. Animals were placed in the center, facing the same open arm. Mice were tested for 5 min and recorded from above using the Viewer 2 tracking software (Biobserve GmbH, Bonn, Germany).

HPLC Analysis of Dopamine, Serotonin, and Metabolites

Animals were sacrificed by cervical dislocation, brains were quickly dissected and striatum as well as substantia nigra were isolated on ice using a mouse coronal brain matrix (CellPoint Scientific, Gaithersburg, MD, USA). Samples were weighed, snap-frozen in liquid nitrogen and stored overnight at −80°C. Tissue was homogenized in 0.4 M perchloric acid using a Sonopuls GM 70 ultrasound homogenizer (Bandelin, Berlin, Germany), centrifuged for 15 min at 20.800 g and 4°C and the supernatant was filtered through 0.2 μm

syringe filter. The filtered postmortem tissue samples were analyzed for dopamine (DA) and its metabolites 3,4-dihydroxyphenylacetic acid (DOPAC), 3-methoxytyramine (3-MT) and homovanillic acid (HVA), as well as for serotonin (5-HT) and its metabolite 5-hydroxyindoleacetic acid (5-HIAA) by high-performance liquid chromatography coupled with electrochemical detection (HPLC-ECD) under isocratic conditions. The detector potential was set at +650 mV using a glassy carbon electrode and an Ag/AgCl reference electrode (BAS MF-1000, Bioanalytical Systems, West Lafayette, IN, USA) at a range of 1 nA/10 V. Injections of 20 μl per sample were done by an auto-cooling autosampler set at 4°C. For chromatographic separation, a reversed phase column was used (100 × 2.1 mm i.d. with pre-column 10 × 2.1 mm i.d., filled with ODS-AQ, 120 Å, 3 μm, YMC Europe GmbH, Dinslaken, Germany). The mobile phase consisted of 1.7 mM 1-octanesulfonic acid sodium salt, 1.0 mM $Na_2EDTA \times 2\ H_2O$, 8.0 mM NaCl, 100.0 mM $NaH_2PO_4 \times 2\ H_2O$, adjusted to pH 3.80 with H_3PO_4, filtered through a 0.22 μm filter, mixed up with acetonitrile (final concentration 9.3% v/v) and was delivered at 0.4 ml/min. For data acquisition and calculation, Chromeleon version 6.5 HPLC software (Dionex, Idstein, Germany) was used. The position and areas of the peaks of the neurotransmitters of interest were compared with external standards using a standard calibration ranging from 10^{-9} to 10^{-6} M. The neurotransmitter amounts were expressed as ng/mg wet tissue weight. For DA and 5-HT turnover, the ratios of (DOPAC + 3-MT + HVA)/DA and 5-HIAA/5-HT were calculated, respectively.

Tyrosine Hydroxylase Staining

Animals were anaesthetized and transcardially perfused with PBS and 4% PFA. Brains were dissected, postfixed for 24 h in 4% PFA at 4°C followed by incubation for 24-48 h in 30% sucrose at 4°C. Brains were embedded in Tissue-Tek O.C.T (Sakura, Leiden, Netherlands) and 40 μm coronal free-floating cryostat sections were systematically sampled throughout the entire brain. Sections were stored in storage solution (1 L PBS, 1 L ethylene glycol, 20 g polyvinylpyrrolidone (PVP)) at 4°C. For staining, sections were washed in PBS, treated with 3% H_2O_2, rinsed with PBS and permeabilized + blocked in 0.3% Triton X-100, 5% goat serum, 1% BSA, 1% PVP for 1 h at RT. Primary antibody anti-Tyrosine hydroxylase (Merck, Darmstadt, Germany) diluted 1:400 in PBS + 1% BSA + 0.3% Triton X-100 was incubated for 48 h at 4°C. After 30 min washing in PBS, sections were incubated 2 h at RT with HRP-conjugated goat secondary antibody (Thermo Fisher Scientific, Waltham, MA, USA), washed again for 30 min in PBS and treated with DAB for color development. Sections were washed, mounted on microscope slides, air-dried and covered with DPX medium (Sigma-Aldrich, St. Louis, MO, USA) and glass coverslips. Images were acquired using a MIRAX Scan (Zeiss, Oberkochen, Germany). Corrected optical density measurement for striatal TH quantification was performed by tracing boundaries of both striata (5 – 8 sections per animal) with ImageJ (NIH) and measuring mean gray levels of inverted 8-bit images. Cortical staining intensities were used for background correction. Because staining intensity varies between different batches, we performed a pairwise analysis of animals stained simultaneously.

TH Cell Counting (Method A)

Number of TH-positive cells were estimated with random sampling of about every third section to yield 5 sections per mouse per substantia nigra (SN). The number of tyrosine hydroxylase (TH) positive neurons was counted in the SN pars compacta (SNpc) of S1/S2 ± dox and V1S/SV2 ± dox mice at 5 months (N = 5 animals per group) and 24 months (N = 6 animals per group). Experimenters were blinded to genotype and treatment. SNpc boundaries were delimited and cell count analysis was automatically performed using open source QuPath software (Queen's University Belfast, UK) (Bankhead et al., 2017). Results were manually verified and corrected if necessary (deleted false-positive, included false-negative). For TH-positive cell count analysis, different layers of SN were categorized into six classes with equal weight (1-6; see Figure S8). Each brain section was assigned to its designated category (1-6) and the cell count was normalized to the mean value of control animals (transgene off) within the same category. For final data analysis, the values per animal over all categories were averaged in order to have one final value per animal, representing the percentage loss/gain compared to control animals.

TH Cell Counting (Method B)

Dopaminergic neurons were quantified by stereologically counting TH-positive cells in the SNpc of the right hemisphere using the optical fractionator method (StereoInvestigator v7.5 ;MBF Bioscience, Williston, VT, USA), a CX9000 camera (MBF Bioscience) and an Axioskop 2 microscope with 40x/0,75 objective (Zeiss, Jena, German). In every fifth 40 μm section spanning bregma levels −2.8 mm to −3.8 mm, neurons were manually identified in 100x100 μm counting frames. The grid size was 100x100 μm, i.e., the entire area of the SN was analyzed. For the V1S/SV2 animals, we stained two sets of sections from each animal (i.e., sections 1, 6, … and 2, 7, …) and averaged the results. Counting was performed blinded for genotype and treatment. For blinding the slides were pseudonymed using intransparent tape by a technician not involved in the analysis.

QUANTIFICATION AND STATISTICAL ANALYSIS

Statistical analysis was performed with SAS (Version 9.4, https://www.sas.com) and Prism (GraphPad Prism Version 6.01, https://www.graphpad.com). Normal distribution of data was tested with D'Agostino & Pearson omnibus normality test, Shapiro–Wilk normality test and KS normality test. Mann–Whitney *U* test (unpaired data) was used for data from non-Gaussian distribution. Paired

t test was used for paired data from Gaussian distribution. 1way ANOVA with Tukey's post hoc test and 2way ANOVA with Tukey's or Sidak's post hoc test were used for multiple comparisons. For behavioral analysis, repeated-measures 2way ANOVA was performed. All tests for significance were two tailed with $\alpha = 0.05$. Statistical details and the meaning of "n" can be found in the figure legends.

DATA AND CODE AVAILABILITY

RNA sequencing dataset of 24 months old V1S/SV2 mice has been uploaded to GEO. The accession number for the sequencing data reported in this paper is GEO: GSE134462.